REVIEWS OF
MODERN PHYSICS

VOLUME 25, NUMBER 4 OCTOBER, 1953

Passage of Heavy Particles through Matter*

S. K. ALLISON,† *Institute for Nuclear Studies, The University of Chicago, Chicago, Illinois*

AND

S. D. WARSHAW, *Argonne Cancer Research Hospital, The University of Chicago, Chicago, Illinois*

I. INTRODUCTION

IF the short summary article by Taylor (Ta52)[1] is excepted, for at least ten years there has been no review published in the periodical literature, either descriptive or discursive by nature, on the subject of experiments in atomic penetration. The present article is therefore intended to remedy this lack, without going into the detailed description of all such phenomena that can be found in the definitive chapter by Bethe and Ashkin in the book, *Experimental Nuclear Physics* (Be53). However, since the closing date on experimental data for that article was 1951, and since at least a few special topics deserve more detail than could be practically included in that chapter, the present article will attempt to supplement it and bring the experimental picture more up to date.

The scope of this article will be limited to the penetration of charged atomic particles through matter, thereby excluding experiments done with mesons or electrons. From the point of view of theory, this is not an important distinction, since except for a few special modifications the accepted basic theory is as good for one kind of charged particle as another. However, it is just these modifications which also make the experimental techniques—between the use of protons and electrons for example—different enough to warrant a separate writing. Those theoretical topics pertinent to the measurement of penetration parameters, the value of these parameters, and factors affecting the accuracy or interpretation of the experiments, will first be discussed; this will be done at the risk of repeating other reviews, but is included for the sake of coherency. There will first be a general discursive section on the phenomena involved; this will include discussion on stopping by ionization of a medium with presentation of the Bethe-Bloch equation and of its validity; discussion of range relation and definitions and calculation from stopping power; the general effects of fluctuation phenomena; a short presentation of some phenomena that are not related directly to ionization of single atoms, but affect the penetration to a more or less significant degree depending, e.g., on the energy of the incident particle: polarization of the medium, charge exchange phenomena, chemical binding, scattering, etc.

As remarked above, Taylor has reviewed the 1952 status of range-energy relations and has included an extensive bibliography; therefore, this article will not attempt to present a comprehensive coverage of the literature (except for work completed since Taylor's article and prior to June, 1953). The usefulness of the range-energy relations, as such, becomes small in the low-energy region, since the preparation and storage of suitable absorbing foils, while possible, becomes a major undertaking. Therefore, the discussion of experimental work in this article will be split into two parts: "low energy," or less than an arbitrarily set 2 Mev (protons), and "high energy," or greater than 2 Mev. The range-energy relations will be given only casual mention in the low-energy part, while measurements on absolute stopping powers will receive brief treatment in the high-energy part. The point of view for the high-energy sections will be that of the experimenter who wishes to determine beam energy and energy spread by means of absorption curves.

* Closed June, 1953.

† Member of National Research Council Committee on Penetration of Charged Particles in Matter.

[1] References in parentheses are given in the Bibliography.

II. DISCUSSION OF PHENOMENA

A. Physical Basis of Stopping

While the physical basis of the stopping phenomena has been well understood for some time (Bo48), discrepancies between theory and experiment can be ascribed to the mathematical difficulties involved in an accurate collision theory. Stated concisely, the problem is: a charged particle with a given kinetic energy passes through a region containing atoms of one kind or another. What is the energy of this particle when it leaves the region? An obvious simplifying assumption is first to consider the region as made up of many isolated atoms, calculate the contribution of a single incident particle-atom collision, and then sum over all atoms. This approximation will turn out to be justified for all but the highest velocity incident particles. In the second place, the numerical value of such a sum must be interpreted as some kind of average value, since each collision will lead, not to some definite, final state of the collision pair, but rather to a probability describing that state; hence, the kinetic energy of the particles in a beam that has passed through such a region will be distributed according to the laws of chance, and for a completely unambiguous interpretation, the essential parameters of this distribution (the "straggling") must be known. Having granted that collisions of the incident particle with single atoms can be summed in an interpretable way, it must still be assumed that the incident particle retains its identity and description: an incident proton can pick up an orbital electron and spend some of its time as a neutral atom at low energy or be lost through a nuclear reaction at high energy.

The collision occurring between one of the atomic electrons and the passing particle (the energy transferred to the nucleus being—usually—small) is considered in the actual calculation of the energy transferred to an atom by ionization. For this calculation the Born approximation may be used: obtain the matrix element for an electronic transition (induced by the field of the passing particle) to a given final state, average over all initial and final electronic states, and then sum over all electrons in the medium. Since the chance that the final electron state will be in the continuum is large, and since these states are easily observable as ionization current, the stopping process is said to produce ionization energy loss. However, part of the energy of the incident particle clearly goes to electronic transitions between discrete states, with the subsequent emission of photons; indeed, after the moving particle has lost so much energy that it has little chance of ionizing an atom, it still moves far enough to produce many atoms in excited states. For this reason the observed range (defined below) will differ according to the type of detector used: an experiment that measures ionization (e.g., with an ionization chamber) will give a slightly shorter range than one using, say, a scintillation counter, which responds to excited atoms. The assumptions made for the Born approximation are that the change of momentum during the collision be small, which can be shown (Mo49, Bo48) to reduce to the condition that Zv_0/v is much less than unity, where $v_0=e^2/\hbar$ is the Bohr velocity, or, in energy units (for protons), that E in Mev is greater than $0.025Z^2$. Hence, for all but the lightest elements (Z less than 10) the low-energy (proton E less than 2 Mev) application of the theory, even ignoring such extraneous effects as charge exchange, is quite dubious. At very high energies, in the full relativistic form the formula would predict a continuous increase in the rate of energy loss, but for the breakdown of the approximation of isolated atoms in the stopping material. For collisions at distances larger than atomic dimensions, some account must be made of the effect of neighboring atoms of the stopping material; polarization of the entire medium by the incident particle produces a decrease in the field of this particle that is effective in the transfer of energy, with a consequent decrease in the energy loss. However, since the distant collisions play an important role only at high energies, in the nonrelativistic case there should be only a small effect, with the important exception of stopping in materials containing a large fraction of conduction electrons. The polarization phenomena should be expected to become significant (A.Bo49) when $mv^2\gg\hbar\omega_A$ (where $\omega_A{}^2=\omega_a{}^2+(1-\alpha)\nu^2$, ω_a corresponding to the binding energy of an isolated atom, $\alpha\gtrsim 1$ a numerical constant, and $\nu^2=4\pi ne^2/m$, with n the electron density). Thus in the case of the light elements (beryllium, carbon), there can be a relatively large effect even at moderate energy. At extremely high energy the effect of polarization is to make the stopping power a constant function of energy rather than a continuously increasing one. (See Be53, Fe40, Ha48, Sc51, St52).

B. Simple Theory of Stopping

The theoretical factors most generally applicable to experimental use are the mean range, the average rate of energy loss, the specific ionization, and the straggling parameter; these are all related in a fairly straightforward way, this being made clear from the simplified classical theory, in which the differential cross section for the transfer of energy between T and $T+dT$ is

$$d\sigma=\frac{2\pi e^4z^2}{mv^2}\frac{dT}{T^2}, \tag{1}$$

where e is the electronic charge and z is the atomic number of the incident particle. Thus, the average rate of loss is obtained by integrating the product $Td\sigma$ (the maximum value being $T_m=2mv^2$, the minimum of the order of the mean excitation potential I) over all possible transfers, the specific ionization by integrating $d\sigma$ over all transfers that result in a free electron-ion pair, the mean square deviation in energy loss by integrating $T^2d\sigma$ over all possible transfers, etc. The mean range

is obtained in a simple way from the mean rate of loss as

$$R_m=\int_E^0 dE(dx/dE). \tag{1'}$$

The mean square deviation from the mean range (if we assume that the distribution is Gaussian) can be shown to be (Bo48)

$$\sigma_R^2=\int_0^E P(dE/dx)^{-3}dE, \tag{2}$$

where $P=4\pi ne^4z^2$.

Actually the distribution in energy loss is not strictly Gaussian, but is rather such that greater losses than the most probable are favored, when collisions between particles of the same order of magnitude of mass are considered as contributing to the net loss. Thus, the ionization loss of electrons or the nuclear collision loss for protons leads to a distinctly non-Gaussian distribution. However, in the high-energy range, nuclear collisions contribute little to the stopping and for the electronic collisions the most probable and the average energy loss are very nearly identical. If one uses the accurate quantum-mechanical theory, the result of the integration over all possible energy transfers gives the average rate of loss as (Li37)

$$-\frac{dE}{dx}=\frac{4\pi e^4z^2}{mv^2}N\left[Z\left(\log\frac{2mv^2}{I}-\log(1-\beta^2)-\beta^2\right)-C_K\right], \tag{3}$$

where the relativistic correction term has been included. In Eq. (3): N is the number of atoms of the stopping material per cubic centimeter; z is the atomic number of the incident particle; Z is the atomic number of the stopping material; β = particle velocity/velocity of light; $C_K(1/\eta)$ is a correction term for binding in the K shell (see below); and

$$\eta=\frac{mE}{M(Z-\sigma)^2Ry}=[v/(Z-\sigma)v_0]^2,$$

where $v_0=e^2/\hbar$, with σ a screening constant (approximately 0.3 for light elements) such that $(Z-\sigma)e$ gives the effective source strength of the field in which the K electrons move. Here I, the mean excitation potential, is a measure of the least (on the average) energy that can be transferred to a bound electron. A good part of the experimental work in the field has been concerned with measurements of I, which is assumed to be a velocity independent parameter and shown by Bloch (Bl33) to be proportional to the atomic number Z for high Z materials. In terms of more easily calculable constants the first factor in (3) can be written

$$8\pi a_0^2Ry\cdot z^2NZ\frac{Ry}{E}\cdot\frac{M}{m}\cdot\frac{\gamma^2}{1-\gamma},$$

TABLE II-1. $C_K(1/\eta)$: Correction for K-shell binding in light elements.[a]

Proton energy Mev	$\frac{1}{(Z-0.3)^2\eta}$	C_K Be	C	Al
0.6	0.0414	0.895	0.900	···
0.8	0.0311	0.780	0.972	···
1.0	0.0248	0.680	0.981	···
1.2	0.0207	0.596	0.951	···
1.4	0.0177	0.531	0.901	···
1.6	0.0155	0.475	0.852	0.380
1.8	0.0137	0.421	0.800	0.552
2.0	0.0124	0.390	0.758	0.613
2.2	0.0113	0.359	0.716	0.700
2.4	0.0104	0.330	0.678	0.767
2.6	0.0096	0.310	0.638	0.820
2.8	0.0087	0.288	0.597	0.861
3.0	0.0083	0.270	0.570	0.892
4.0	0.0062	0.208	0.451	0.975
5.0	0.0049	0.160	0.361	0.880[b]

[a] From the curve of Fig. 2 in M. C. Walske, Phys. Rev. **88**, 1283 (1952), for the three elements θ_k was taken as 0.7. The last decimal is, of course, doubtful.
[b] Above this energy the correction in Al is less than 1 percent.

where M is the rest mass of the incident particle, a_0 the Bohr radius, γ the Lorentz factor $1/(1-\beta^2)^{\frac{1}{2}}$, and E the kinetic energy.

In the low-energy range, the Born approximation for heavy materials would fail, since the inner electrons move at very high velocities compared to the incident protons, and a correction for binding in the inner electron shells must be applied. This is done by subtracting the number C_K from the logarithmic term in the Bethe-Bloch formula. These corrections have been calculated most recently by Walske (Wa52) and earlier by Brown (Br50), and still earlier given by Livingston and Bethe (Li37) in their 1937 review; in all of these, the correction is given as a function of the particle velocity in units of K-shell electron velocity.‡ Some representative values from Walske's article are given in Table II-1.

The Bethe-Bloch equation then stands as an approximation valid in a restricted energy range (which differs for different particles and materials) and requiring the measurement of a parameter, the mean excitation potential; further, this parameter is velocity dependent, at least at high energy, because of polarization phenomena (and incorporating this effect into the excitation potential), although at most energies it is relatively constant except for binding corrections.

For protons in the energy range 20 kev to about 2 Mev, there is no satisfactory theory, and recourse must be made to empirical data. Below 20 kev the statistical theory of Fermi and Teller (Fe49) has not been directly verified (however, see Sec. III). In heavy materials, a crude statistical argument (Bo48) gives a $Z^{\frac{1}{2}}/v$ dependence of the stopping power at lower energies. Experimental agreement with this is only qualitative (Wa49).

‡ It should be pointed out that in the widely used tables calculated by Aron (Ar51) the wrong C_K correction was evidently used: instead of calculating the ratio v/v_K, Aron apparently used four times this value.

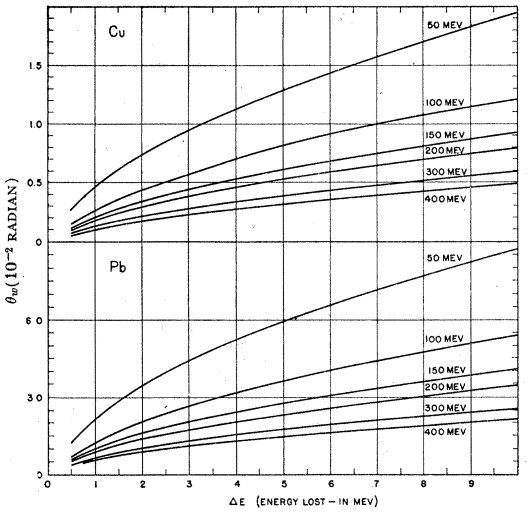

(a)

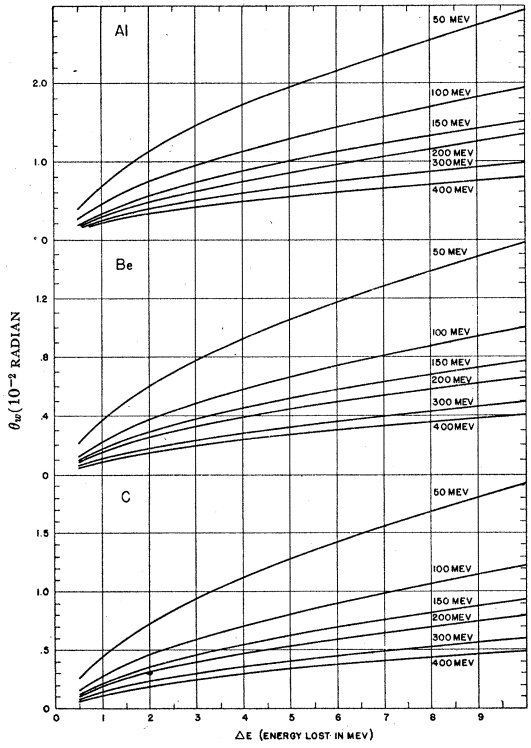

(b)

FIG. 1(a+b). The effective rms (unprojected) scattering angle θ_w as a function of energy lost in the scattering material.

Experimentally, the measurement of range may be done by obtaining the curve for the number of particles remaining in a beam as a function of the thickness of the material the beam has to pass through and identifying a point on that curve with the mean range. By definition this point would be the thickness R_m of material for which one-half of the particles have been absorbed by the ionization process; the ideal absorption curve for monoergic protons would have such a form that the derivative dN/dx, where $N(x)$ is the number of particles counted for absorber thickness x, would be a Gaussian. However, in practice this is almost never the case. If the mean range is defined as above, such that one-half of the incident beam travels a distance greater than R_m and one-half less than R_m, then clearly because of small-angle multiple scattering of the beam (that is, angles small enough so that the detector still sees the entire beam) the observed mean range being the projection of many short segments of trajectory, each randomly oriented to the axis of the beam, will be smaller than the "true" mean range. The effect of scattering is most significant, of course, near the end of the range. Following Mather and Segrè (Ma51) the difference between observed and true ranges may be written as

$$R_{\text{obs}}=\sum_i l_i\cos\theta_i \doteq \sum l_i\left(1-\frac{\theta_i^2}{2}\right)=R_m-\tfrac{1}{2}\sum l_i\theta_i^2, \quad (4)$$

where l_i is the distance between the ith and $(i+1)$th small angle collision, and θ_i the direction with respect to the beam axis after the ith collision. An approximation of the value of θ_i was obtained from William's formula (Wi45),

$$\langle\theta_i^2\rangle=\frac{Zm}{M}\log(E_0/E_i). \quad (5)$$

By assuming that R is roughly proportional to $E^{1.75}$, writing the sum as an integral and integrating, we get $(R_m-R_{\text{obs}})/R_m=Z/6440$. It is, therefore, of the order of 1 percent for copper.

Other authors (Bl51) have used somewhat more accurate expressions for the mean square scattering angle with a resulting formula for the range correction that differs in form from the above expression but only by a

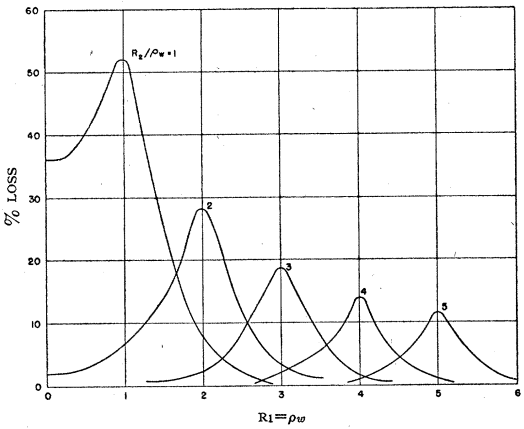

FIG. 1c. From reference Di53: Fractional beam loss as a function of detector and source geometry; R_1=source radius; R_2=detector radius; $\rho_w=S\theta_w$, with S=source-detector distance.

small amount numerically. This is

$$\langle\theta^2\rangle=\int_{-R_m}^{-x}ZPG(pv)^{-2}dx, \tag{6}$$

where P is defined above, $G=2\log 181Z^{-\frac{1}{3}}$, x is the residual range, and p, v are the momentum and velocity of the incident particle. The range correction is then $\delta R/R=ZPG/C$, where it has been assumed that $(pv)^{-2}=Cx$. For Al, $C=2.6\times10^{-8}$, for Cu, $C=8.9\times10^{-8}$. A full discussion of the multiple scattering theory (Ro41, Gr50, Sc50, Mo51, Be53) is beyond the scope of this paper. The correction is, in most cases, small, and relatively large errors in the correction are of little consequence. However, for aid in the interpretation of some experiments, it is useful to have an estimate of the beam spread as it is passed through relatively thin targets. To this end we have calculated curves for the mean square angle of scatter (at several high energies) as a function of the energy lost in the target, using an approximate form of Moliere's (Mo51) expression for the scattering angle, and Aron's table for the energy loss. Both of these are sufficiently accurate for this purpose. Moliere's expression gives an angle which is not properly identified as the spread of a Gaussian distribution in scattering angles. His distribution function has a leading term which is Gaussian, but there are also higher order terms (making the resulting curve slightly greater for small angles and smaller than Gaussian at larger angles) resulting from a smooth transition from multiple to single scattering. Following Hanson, *et al.* (Ha51) let θ_w be the $1/e$ width of an effective Gaussian distribution, fit to Moliere's theory. Then as given in (Ha51)

$$\theta_w^2=\theta_1^2(B-1.2), \tag{7}$$

where

$$\theta_1^2=\frac{4\pi NZ(Z+1)xe^4}{p^2v^2},$$

$$\theta_a^2=\left(\frac{\hbar Z^{\frac{1}{3}}}{0.885pa_0}\right)^2\left[1.13+3.76\left(\frac{Z}{137\beta}\right)^2\right],$$

x is the thickness of the stopping material, and $B(\theta_1/\theta_a)$ is the auxilliary function tabulated by Moliere (see also reference Be53). The group of curves in Fig. 1 gives θ_w for several elements and energies. In this connection, the evaluation of particle loss resulting from the multiple scattering that has been made by Dickinson and Dodder (Di53) is of interest. Figure 1(c) gives the calculated fractional loss as a function of detector radius R_2, the foil radius R_1, and the average normal displacement $\rho_w=S\theta_w$, with S the foil-detector distance. (These curves were actually calculated with Moliere's $\langle\theta^2\rangle_{Av}$, but the difference, for this application, is negligibly small.)

At higher energies, nuclear collisions may occur which attenuate the beam intensity, thereby changing the shape of the absorption curve, and thus the point corresponding to the mean range. If N_0 is the initial beam flux, then R_m would be the thickness x of the absorber for which the flux N is $\frac{1}{2}N_0$; if the fraction f is attenuated, $1-f$ remaining, then this point should be at $(1-f)N_0/2$. The fraction f may be calculated from the data of Kirschbaum (Ki52) which is shown in Fig. 2, giving σ_{abs} as a function of the nuclear mass A. In Kirschbaum's work, the cross section was measured by observing the average slope of the integral absorption curve for a beam of protons passing through a variable thickness of absorbing material. The point just to the left of the knee of the curve was taken as the running point for attenuation measurements. The cross section is then given at the average energy of the beam in the attenuator. The significance of this type of measurement in the interpretation of nuclear reactions is beyond the scope of this work, but the use of this technique makes the results directly applicable to the correction for range. (Also on Fig. 2 the data of Perry (Pe51) and Bernardini, *et al.* (Be51) are shown, with some evidence of a different slope.) While an exponential fit to the energy variation probably has no theoretical significance, for present purposes it is convenient to represent Kirschbaum's data by the empirical relation $\sigma_{abs}=\sigma_0\exp(-E/\epsilon)$, where $\sigma_0=\pi r_0^2A^{\frac{2}{3}}$ is the geometric cross section ($r_0=1.37\times10^{-13}$ cm) $\epsilon=400A^{0.14}$ Mev, and E is the average energy of the protons in the attenuator. The absorption curve is very steep near the end of the range so that the range will be insensitive to rather large errors in the determination of $f\doteq0.9R_m\sigma_{abs}$, where R_m is expressed in atoms/cm^2 and the factor 0.9 gives an approximately correct "running point." Included in f, of course, should be the contribution from large angle Coulomb scattering, which will depend on the geometry of the experimental arrangements.

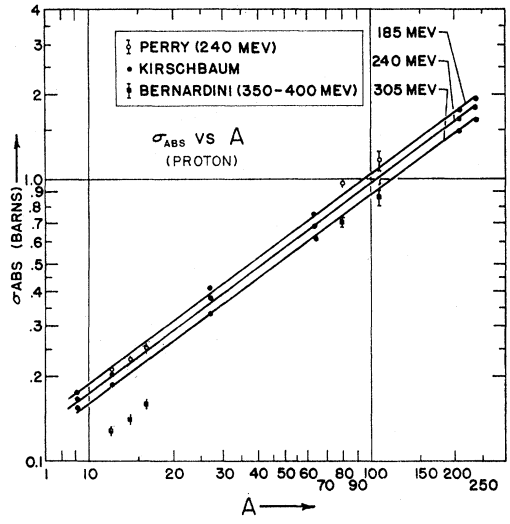

FIG. 2. Experimental high-energy nuclear absorption cross section (for protons) *versus* atomic weight.

C. Fluctuation Phenomena: Straggling

The statistical nature of the stopping produces also a fluctuation in the distance traveled by the incident particle before being stopped as well as a corresponding fluctuation of the total energy loss by the particle. This is because the number of collisions necessary to reduce the particle energy to zero will vary, since the energy that may be transferred in a single collision is distributed between a minimum and a maximum value. For incident electrons, *all* of the energy may be transferred in a single collision, so that the distribution in range may show many particles with very small range; for protons the maximum is only about 1/460 times the initial energy, so that the differential range distribution should be sharp and nearly Gaussian. The standard deviation, σ_R, from the rectified mean range due to straggling was obtained experimentally by Mather and Segrè (Ma51) by measuring the Bragg ionization curve for 340-Mev protons in various materials; the mean range was obtained by assuming a Gaussian distribution of range about the mean, with a spread measured by σ_R, and by fitting this curve to the measured curve near the end of the range. They found that the center of the Gaussian fit the data best where the ionization was 0.82 times its maximum value. For elements from Be to Pb, $\sigma_{R(\text{exp})}$ varied from 0.91 to 1.90 g/cm^2, while the theoretical value $\sigma_{R(\text{theoret})}$ (see above) varied from 0.65 to 1.35. The difference was attributed to a small but significant energy spread in the initial beam which was then calculated to be 0.5 percent. These authors also found that the distribution was not truly Gaussian, but rather slightly skewed toward shorter ranges.

The same group had earlier measured $\sigma_{R(\text{exp})}$ in copper and again determined that agreement with theory was good if the beam spread was only about 0.5 percent. In the same year Bloembergen and Van Heerden (Bl51) determined the straggling parameter s, for protons from above 35 Mev to 115 Mev in lead, aluminum, and copper from integral range curves. The parameter here is defined as the difference between the mean and extrapolated range, where the extrapolated range is determined by the intercept with the R axis of the tangent drawn on the absorption curve at the $N_0/2$ point. Comparison with theory was made by calculating $\sigma_{R(\text{theoret})}$, including the effect of multiple scattering as well as the range straggling effect; σ_s, the contribution from scattering, is a function of the mean square deviation of the normal angle from the beam direction near the end of the range. The quantity $(\sigma_s^2+\sigma^2_{R(\text{theoret})})$ agreed well with $\sigma^2_{R(\text{exp})}$ with σ_s calculated from the formulas given by Livingston and Bethe (Li37). (It should be noted that S is related to σ_R by $S=(\pi/2)^{\frac{1}{2}}\sigma_R$ if a Gaussian is assumed.)

The value of the range straggling is generally small. Using the value for σ_R given above (Eq. 2) and substituting from the Bethe-Bloch formula, while neglecting the variation of the logarithmic factor, one finds

$$\frac{\sigma_R^2}{R_m^2}=\frac{4m}{M}\cdot\frac{1}{\log(2mv^2/I)} \tag{8}$$

for light stopping materials, and

$$\sigma_R^2/R_m^2=3m/4M \tag{8'}$$

for heavy materials, where m/M is the ratio of electron to incident particle mass. These relations have been verified for practical purposes (the straggling is of the order of 1 percent) by Madsen and Venkateswarlu (Ma48) at low energy. At high energy, Tobias (To51) using 190-Mev deuterons in aluminum finds a straggling effect of 0.017 or about twice the theoretical value given by Wilson (Wi47) in the expression,

$$\sigma_R/R_m=0.24(E/Mc^2)^{-0.1}(Mc^2)^{-\frac{1}{2}}, \tag{9}$$

which was derived by approximating the logarithmic factor above with a power function (Mc^2 = rest energy of proton in Mev).

The extrapolated range may be expressed in terms of the mean range and the straggling parameter by expanding $R(N)$ in a Taylor series (where unit flux is incident);

$$R(N)=R_m+(N-\tfrac{1}{2})\left(\frac{dR}{dN}\right)_{N=\frac{1}{2}};$$

if a Gaussian of spread σ_R is assumed, then

$$R(N)=R_m+\left(\frac{\pi}{2}\right)^{\frac{1}{2}}\sigma_R. \tag{10}$$

The slight amount of skewness found by Mather and Segre can, perhaps, be quantitatively explained by the calculation of Caldwell (Ca52) who obtained (using the work of Lewis (Le52)) values for the theoretical integral range distribution of fast (2–500 Mev) protons in aluminum to show how the distribution differs from Gaussian. The difference is small: for 200-Mev protons in aluminum, the lengthening of the mean range because of this is only 0.021 percent. Since, however, this calculation is better than the range straggling curves published in previous reviews, Caldwell's curve is reproduced here (Fig. 3).

The energy loss straggling theory has been worked out by Landau (La44) and improved by Blunck and Leisegang (Bl49); these authors give the distribution in energy loss for not too thick slabs of stopping material. A first approximation to the loss straggling is given by Bohr (Bo48) as the spread of a Gaussian distribution, with the resulting spread independent of particle velocity; this neglects the effect of collisions which, though infrequent, result in relatively large energy transfers and produce a tail on the loss curve favoring larger loss. This corresponds to the tail on the

range distribution mentioned above, with shorter range favored. The distribution given by Landau contains this effect, which, however, is small enough so that most conventional energy measuring equipment is not able to resolve the components contributing to the smear. Using a calibrated proportional counter with pulse-height discrimination, and 32-Mev protons, Igo, Clark, and Eisberg (Ig53) were able to show the "Landau" effect in fair agreement with their measurement. Experiments with electrons verify this distribution and the effect is much more striking (see Be53). At lower proton energy, the simple Bohr formula is a fair approximation for "not too thin" (but not thick enough to make a large energy loss) absorbing foil. This has been shown by Madsen and Venkateswarlu (Ma48b) working at energies under 2 Mev with beryllium and mica as foils and using the resonance radiation from aluminum and fluorine targets as energy indicators (see Sec. III).

While in principle the measurements of absolute stopping power with finite resolving power equipment should be corrected by a fold of the resolution curve in the Landau distribution or some other appropriate distribution, the corrections at high energy are shown to be small, and therefore the fold has not been made. At lower energies somewhat simpler techniques have been used; these will be discussed in the section on results of measurement in the low-energy region.

D. Other Related Phenomena

At the extreme low-energy end of the picture, the increasing dominance of collisions of the incident particle with entire atoms of the stopping region, large-angle Coulomb scattering, and charge exchange phenomena make experimental determinations of the range in even gaseous materials rather uninterpretable. While the range in centimeters can be extended at will by using the gas at variable pressure, the first two effects produce large energy loss and hence a large range straggling, with no resulting ionization, and reduce the precision enormously. Furthermore, loss by ionization is becoming less important since the effective charge of the moving particle (see below) is approaching zero as electrons are picked up.

1. Charge Exchange Phenomena

Although charge exchange phenomena are properly a separate subject for discussion from stopping or range relations—with which this article is largely concerned—in order that low-energy experimental data on stopping be understood, it is necessary that some attention be paid to the charge state of the incident beam. Furthermore, while very early work in this field has been published (see, for example, reference Ru33), much of the early results failed to give quantitative or reproducible values for the parameters involved in the theory. More recently, interest in this field has been stimulated by

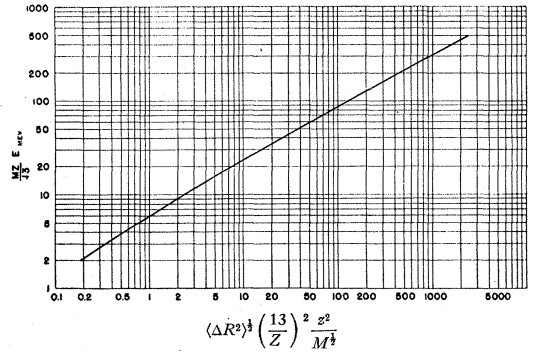

FIG. 3. Curve from reference Ca52 for the straggling about the mean range as a function of energy. Z is the atomic number of the stopping material, z of the incident particle; and M is the ratio of particle to proton mass.

studies of the ranges of fission fragments, in which case the charge exchange collisions and "hard" collisions play an important role. The practical desire of experimentalists to obtain multiply charged ion beams for accelerators has also stimulated recent work. Therefore a brief description of the existing theory of charge exchange will be given in this section and a fairly complete summary of recent measurements (performed largely by the Chicago group) will be given in Sec. III, on low-energy measurements.

A proton moving through material can capture an electron into a bound state; subsequent to this capture, the moving hydrogen atom can then lose its electron, the experimental picture then being one in which stopping power measurements are being made with a "particle" that is sometimes a singly charged proton and the remainder of the time a neutral system with a relatively widely separated proton-electron pair. If the cross sections for capture and loss were known, the relative fractions of time that the system is in either of these states could be calculated, and if the effective stopping power of the neutral system can be determined, then the measured energy loss of an incident low-energy proton can become interpretable. Thus, using a simple estimate for the stopping power for a neutral hydrogen atom§ and estimates of the cross sections for capture and loss given by Bohr (Bo48), Warshaw (Wa49b) argued that except where the capture cross section (σ_c) and the loss cross section (σ_l) become nearly equal—for proton velocity approaching v_0, about 25-kev energy—Eq. (3) could be used without introducing any essential modification from this source at least. Indeed, it has been argued by Isenberg (Is50) that bound states of hydrogen atoms in metals cannot exist, which would make the motivation

§ The effective charge for the neutral atom will be zero for distant collision, impact parameter≫Bohr radius. For the close collisions, the effective field of the electronic collision partner will be screened by the bound electron of the hydrogen atom. The choice (stopping for H^0) = 0.46 (stopping for H^+) corresponds to an effective electronic charge of about $0.7e$ (i.e., a "screening constant" of about 0.3). The estimate was made, however, by actually using, in the matrix element for the energy transfer, the potential of the ($1s$) hydrogen atom, rather than of a bare proton.

for such an analysis also nonexistent, except for the case of stopping in gases. The case of the stopping of highly charged, massive particles like fission fragments has been discussed by Knipp and Teller (Kn41) and most recently by Bell (Be53a) who obtained values for the effective charge of the fragments and compared the results with recent experiments.

Bohr has pointed out that for heavy stopping materials, those electrons will be captured whose orbital velocities are comparable with v, the incident particle velocity, in which case neither the classical nor the quantum-mechanical (Born approximation) calculation is accurate. However, to obtain an order of magnitude, Bohr applies Eq. (1) and using a statistical argument to select those electrons which, after a collision result in their removal, will be captured into any bound state, he estimates

$$\sigma_c = 4\pi a_0^2 z^5 Z^{\frac{1}{3}} (v_0/v)^6. \tag{11}$$

References to more accurate early calculations for capture cross sections have been listed by Hall (Ha50). Of these, that by Brinkman and Kramers (Br30) gives a variation like v^{-12} for capture from a $1S$ state into a $1S$ state for $v \gg v_0$. In an actual experiment, of course, capture need not be $1S \rightarrow 1S$, and the sum over the different possibilities (Mo49) modifies the exponent to a smaller value. However, as will be shown in Sec. III, the Brinkman-Kramers theory gives much too large values, a discrepancy which can be attributed to failure of the Born approximation in the experimental energy region (Ri52), but which, as has been pointed out by Bates and Dalgarno (Ba52) and Jackson and Schiff (Ja53), is more likely caused by an incorrect choice of interaction potential. The first authors do not include the contribution to the cross section for capture into excited states, and while their energy variation is nearly what is observed, their magnitude is about 1.5 times too small. Jackson and Schiff do, however, obtain quite good agreement with experiment.

The loss cross section can be estimated more directly, the problem being essentially that of the ionization energy loss, but now in a coordinate frame moving with the incident particle. Again using Eq. (1) and integrating over the range $I_b < T < \infty$, where $I_b = z^2 Ry$ is the binding energy of the electron, one gets

$$\sigma_l = 4\pi a_0^2 Z(Z+1) z^{-2} (v_0/v)^2, \tag{12}$$

where the term linear in Z can be shown (Bo48) to account for the nuclear interaction. This formula is to be viewed as good for light stopping materials. Bohr argues that for intermediate Z materials, where screening may play a dominant role, one gets, to an order of magnitude

$$\sigma_l = \pi a_0^2 Z^{\frac{2}{3}} z^{-1} (v_0/v). \tag{12'}$$

Thus it is expected that for protons the ratio $\sigma_l/\sigma_c \sim Z^{\frac{1}{3}} E^{5/2}$, i.e., nearly independent of Z and rapidly increasing for $E \gtrsim 25$ kev. This is actually rather close to what is observed.

2. *Collisions with Nucleus*

For the *nuclear* stopping contribution to energy loss, the classical theory (Bo48) may be applied. Since the transfer of energy to a single heavy nucleus can be a large fraction of the proton energy, a distribution in loss more nearly like the Landau type (La44) than Gaussian may result. No measurements seem to be available at present which could refer specifically to the nuclear stopping contribution; for particles as light as protons and alpha particles, nuclear stopping effects play a very subordinate role, becoming significant, however, for more massive particles like fission fragments (Bo48, Bø40).

3. *Chemical Additivity; Effect of Phase of Stopping Substance*

This discussion of related phenomena will conclude with a short discussion on the stopping properties of compounds. Much of the experimental work has been stimulated by studies of the effect of radiation on living systems, in which the energy absorption takes place in a medium containing several atomic species. It is then necessary to inquire whether the average absorption can be represented as a sum over the different atoms even when these are chemically bound to each other. If strict additivity were correct, the stopping power could be represented—adding energy increments along the path—by Eq. (3) with an effective ionization potential, defined by

$$\log I_{\text{eff}} = \frac{\sum a_k Z_k \log I_k}{\sum a_k Z_k},$$

where the compound has the formula $A_{a_1}{}^1 \cdots A_{a_k}{}^k \cdots A_{a_N}{}^N$. In at least one theoretical calculation for the stopping properties of compounds (Hi38) the use of the additivity property has been indicated. Several measurements at low energy and one measurement at high energy differ on the presence or absence of the additivity rule. The careful work by Thompson (Th52), using 340-Mev protons from the Berkeley cyclotron and a variety of organic compounds (containing C, H, O, N, and Cl) as targets to slow the protons to 200 Mev, shows that to at least 1 percent the relative stopping power is additive; however he found small (i.e., less than 1 percent with a stated experimental precision of better than 1 part per 1000) but measurable deviations from the additivity rule, these deviations depending, for example, on the molecular structure of the compound (see Table II-2). In Thompson's work relative stopping ratio $S = (R/A)_{\text{Cu}}/(R/A)$, where A is the atomic weight and R the range in grams per square centimeter. This is a molal stopping power relative to copper and he shows that, theoretically, for the compound $A_a B_b$, $S = aS_A + bS_B$, and is nearly independent of energy as long as the Bethe-Bloch equation is valid. The conventionally defined relative stopping power is the ratio of stopping cross sections (energy loss per atom per unit area) generally relative to air.

Another recent measurement of the stopping by compounds has been that of Wenzel and Whaling (We52, also Fr51) who obtained the stopping cross section in the low-energy range (20 to 500 kev) of D_2O ice to about 4 percent accuracy; this measurement disagreed with previous measurements (Cr42) taken on D_2O vapor but does agree with the Hirschfeld and Magee calculation for water. These authors conclude that additivity might be indicated except for the uncertainty in the knowledge of theoretical values; they point out that there is evidence that the stopping depends on the phase of the stopping material (that is the assumption of isolated noninteracting atoms is not valid). However, the theory shows that there should be little effect on the stopping due to molecular binding, hence (except for polarization phenomena which would cause denser media to be less effective, per unit mass, than the equivalent gases, but only slightly) there should be no difference between the phases. Several measurements with alpha particles in water, including the old experiments of Michl (Mi14) and Phillip (Ph23) and the more recent measurements of Appleyard (Ap51), show a difference between condensed and vapor phases of about 15 percent. These experiments have been criticized by de Carvalho and Yagoda (Ca53) who, using a photographic method, concluded that the difference between water and ice stopping properties is nonexistent, and that the measured relative stopping power for each agrees with an additivity theory. They give the measured integral molecular stopping power of H_2O as 1.56 ± 0.02 at 5.3-Mev alphas, and for RaC′ alpha particles as compared with a computed 1.54. Other evidence favoring the additivity rule is given by Ellis, Rossi, and Failla, (El52) who measured and compared the stopping power of CH_2, in thin foil and gaseous form. They used Po alpha particles and, after passing these through acetylene gas to a windowless ionization chamber, interposed a foil of polystyrene and observed the changes of ionization. Within the experimental uncertainty of about 5 percent, the indication is that the stopping properties of solid and gaseous phases are equivalent. Furthermore, the measured stopping power agreed with theory.

TABLE II-2. Effective stopping power of bound elements.[a]

Element	Binding	Molal stopping rel. to Cu	S mass stopping rel. to Al[b]	I_{eff}[c] ev
H	Saturated	0.04797±0.0007	2.647	15.3
	Unsaturated	0.04879±0.0001	2.692	12.8
C	Saturated	0.24627±0.0002	1.141	67.6[d]
	Unsaturated	0.24674±0.001	1.143	66.5
	Highly chlorinated	0.2509 ±0.0008	1.162	57.5
N	NH_2, NO_3	0.2785 ±0.0025	1.106	88.5
	in ring	0.2870 ±0.002	1.140	68.1
O	−O−	0.3187 ±0.002	1.108	87.6
	O=	0.3226 ±0.001	1.122	78.6
Cl	All	0.6335 ±0.004	0.994	151.9

[a] From Thompson's thesis, UCRL-1910.
[b] Converted from molal stopping power, using Cu/Al value from Bakker and Segrè, Table IV-1
[c] Using $I_{Al}=151$ ev.
[d] Compare 58.5 ev given by (Pr52).

III. METHODS OF MEASUREMENT AND RESULTS IN THE ENERGY REGION 25–2000 KEV

This section is intended to be a summary of the results of experimental investigations on the stopping power of matter for particles of atomic mass and of kinetic energies in the range 25 to 2000 kev. Following some general remarks concerning range-energy relations in this energy region, part A will deal with the stopping powers of metals and solids, part B will summarize the stopping powers of gases, and part C will deal with experiments on charge exchange.

As already remarked, in the lower part of the energy interval with which this section is concerned, the range measurements begin to lose their usefulness as a method of measuring energy. The stopping powers of solids for the moving particles becomes so great that the preparation of foils through which they can pass, although possible, becomes a major effort in itself (see Sa52 and Gr52), and the use of a set of such delicate foils for range determinations is impracticable. Although the range in centimeters can be extended at will by using a gas at variable pressure as the stopping medium, the "range" in the lower-energy interval becomes noticeably dependent on the geometry. If no collimation of the rays is attempted, the straggling of the range is detrimental to precision. This straggling arises from the increasing dominance of collisions in which the momentum and energy are shared with an entire atom of the stopping medium, producing no ionization but resulting in large energy loss and large change in direction. The loss of energy by ionization of the stopping medium is fading out of the picture because the effective charge of the moving particle, due to electron capture, is approaching zero. Hence, if particles are accepted for range measurement which can have suffered significant deviations|| in direction, an appreciable fraction of their energy loss has occurred by a process in which the loss of energy in a single event is large related to the total energy. Thus, to a certain extent, we approach the behavior of high energy photons in passing through matter, where the entire energy of the photon may be lost in a single event, and one does not speak of a range, but merely of an exponential diminution with distance (St52).

Furthermore, in such uses, the "range" will depend on the method used for detecting the particles. They may retain their ability to eject secondary electrons from a sensitive surface after they have ceased to be able to ionize a gas, and hence their "secondary-electron-ejecting range" may be greater than their "gas-ionization range."

|| See Bo48, definition of θ_a, Pp. 20, 47.

A. The Stopping Power of Metals and Solids for Protons, Deuterons, and Helium Ions

Much of our present knowledge of the stopping power of metals and mica for protons and helium ions in the energy region 25 to 2000 kev arises from a series of experimental investigations carried out at the University of Chicago, in Copenhagen, and at The Ohio State University.¶ The stopping power of D_2O ice has been measured for protons and deuterons in a part of this energy range at the California Institute of Technology (We52).

1. Measurements by the Chicago Group

The investigations at Chicago published by Wilcox (Wi48), Hall and Warshaw (Ha49), Warshaw (Wa49a, b), and Kahn (Ka53), were all carried out in essentially the same manner, using, with small variations, the experimental equipment shown in Fig. 4.

Protons, deutrons, or He^+ ions were accelerated in a Cockcroft-Walton accelerator, for the lower-energy ranges, or, in the case of Kahn's work, in a 2-Mev van de Graaff generator. The desired ionic constituent of the accelerated beam was magnetically sorted and directed to a scattering target, or in some cases to a target giving disintegration particles for which stopping power measurements were to be made. The particles scattered at 90°, or those from the nuclear disintegration, were passed through a compartment in which a foil could be placed in their path at the will of the investigator. On leaving this compartment, the particles passed into a cylindrical electrostatic analyzer in which their energy was determined from the applied potential necessary to bend them 90° and focus them on a slit, behind which was some sort of particle detector.

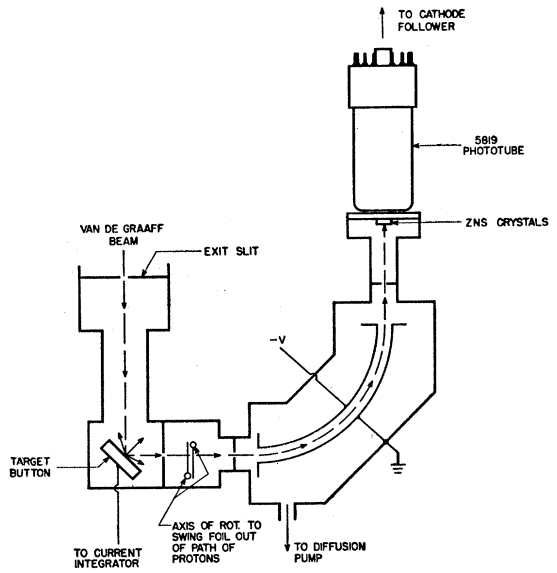

FIG. 4. A typical arrangement used by the Chicago group for the measurement of the stopping power of metal foils.

¶ Chilton, Cooper, and Harris (private communication).

The reason for the use of the scattered beam for passage through the foil rather than the direct beam from the accelerator is essentially a practical one. Although foils which can transmit the direct beam from the accelerator can be produced, they are very apt to be fractured, especially in the preparatory stages of an experiment, in which the beam is being focused, or the accelerator tube is in unsteady operation. There is no necessity to conserve intensity in such experiments, and the loss of it in scattering is unimportant. To avoid loss of homogeneity in energy in the beam on scattering, a very thin, 0.008 mg/cm², layer of gold evaporated on a solid beryllium backing was used. The intensity of scattering from the light beryllium is so low with respect to that from gold that it is negligible, and furthermore the Be-scattered protons only retain 80 percent of their energy (see Wi48, Fig. 2) and are not seen at all in the experiments in which beams are transmitted by foils which remove 10 percent or less of the incident energy.

The procedure for measuring the energy loss was quite simple. With the high-energy ion source in steady operation, the energy profile of the scattered beam was obtained by varying the potential on the electrostatic analyzer; see Fig. 5. The foil was then swung into the scattered beam, and the energy profile of the scattered particles which is transmitted was again obtained. In most cases, the foil was then swung out of the beam and the energy profile run again, to make sure that the kevatron or van de Graaff voltage had not drifted during the "foil in" measurement. The energy loss ΔE in the foil was measured between the ordinates of symmetry of the foil and no-foil curves. Strictly speaking, as Landau (La44) has calculated (see Sec. II) there should not be an ordinate of symmetry in the foil profile even if one exists in the no-foil profile. Kahn (unpublished) investigated his profiles using the results of Landau's work and estimated that the nonrandom error** introduced into his dE/dx values through lack of symmetry in the foil curves was negligibly small compared to errors from other sources, such as determination of foil thickness. By choice of appropriate foils, the energy losses were kept to approximately 10 percent of the original energy.

The major source of error in the Chicago stopping power measurements was the determination of foil thicknesses, which for metals were on the order of 0.1 mg/cm². The early work of Wilcox (Wi48) proved to be mainly valuable in showing, unfortunately in retrospect, that commercially rolled or beaten foils are not always reliable for measurements of the present type (see Ha49 and Wa49b). This point will be returned to later. A technique for the preparation of evaporated

** There is no error introduced at all if the results of measurement are taken to be the "most probable loss" rather than "average loss." The "most probable" will, of course, be slightly less than the "average."

metal foils has been described by Warshaw (Wa49a), as follows:

"Carefully cleaned glass slides were first coated with a weakly adherent plastic film by immersion in a 5 percent solution of pyroxylin in a 50 percent mixture of ether and alcohol; the slide was withdrawn in such a way that the excess liquid could drain off. The concentration of the pyroxylin was not found to be critical, but best results were obtained when the liquid flowed easily, and was still just concentrated enough to form a barely visible coat on the glass when dry. (Pyroxylin is sold as "Parlodion" by the Mallinckrodt Chemical Company.) The coated slide was then placed in a vacuum evaporator, on a wire rack at a convenient distance from the source, and, using standard evaporation techniques (St45), covered with metal. After evaporation, the edges of the film on the glass were roughed with a sharp knife, and the film cut across at about 2 cm intervals. The slide was then immersed at about a 45° angle to the surface of a dish of distilled water. The surface tension of the water was usually enough to peel the plastic film off the glass, carrying the foil with it, and leaving the foil and backing floating on the water surface. If the Parlodion solution was too dilute, the water generally failed to disengage even the edges of the foil; it was then necessary to soak the slide in an ether-alcohol mixture for a few minutes, and free the foil completely by working at the edges with a wire loop forceps. However, if the foil were freed under the surface of the liquid, it generally curled up, indicating that it was deposited in a highly strained state. This, of course, made mounting difficult. Small local strains also developed, very often, around dust particles and water bubbles in the plastic solution; therefore absolute alcohol was used and the solution prepared as dust free as possible and stored in a clean, glass-stoppered bottle.

For mounting the foils, it was convenient to use a small brass frame, about 1.5×2 cm, with a 2 mm wall. This was placed under the floating foil and raised carefully so that the surface tension would not cause any rupture. The last few wrinkles were removed with the aid of a soft brush dipped in alcohol and the foil then washed free of the plastic by dipping it, mounted on the frame, into the ether-alcohol, at right angles to the liquid surface."

Three methods have, at various times, been used by the Chicago group in measuring foil thicknesses.

(a) *Weighing.*—Kahn determined the mg/cm² of his foils by weighing a known area on a microbalance.†† Simultaneously with the deposition of the evaporated metal for the foil proper, a deposit was collected through an aperture of known area on a weighed platinum foil, a subsequent weighing of which indicated, by difference, the number of mg/cm² laid down. The glass microscope slide for the receipt of the foil itself, and the platinum foil were rotated over the source of evaporation many times during the deposition, to insure uniformity of deposit. The deposits were 2.856±0.006 cm² in area, and the error in determining the amount of evaporated metal by weighing ranged from ±1 percent for 200 micrograms of deposit to ±0.5 percent for deposits of the order of 1 milligram.

(b) *Interferometry.*—For this purpose,

"a mirror from a Michelson interferometer was placed in the evaporator bell jar at the same time as the coated slide, and in as nearly the same geometry as possible, but with half the mirror covered by a shield. The deposit of metal on half the mirror then corresponded to the amount deposited on the glass slide. Fringes were obtained with yellow (Na-D) light and the relative displacement of the two sets of fringes—one set from each half of the mirror—then gave the linear thickness of the foil in half wave-length units, after the displacement was first estimated using white light

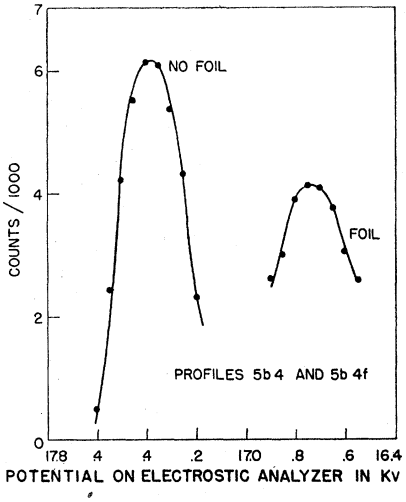

FIG. 5. Analysis of the incident (no foil) beam and the transmitted (foil) beam in the experiments of Kahn (Ka53). The energies of the protons focused on the detector (Fig. 4) are obtained by multiplying the abscissas by 45.23.

to determine the integral number of fringe displacements. It was found most convenient to make an enlarged photograph of the fringes, and determine the displacements from this with a traveling microscope. The probable error, obtained by measuring a large number of displacements separately, was about ±2 percent. The linear thickness was then converted to mg/cm² by using the usual bulk density of the metal."

The use of the bulk density for the conversion of the interferometric thickness to mg/cm² may be questioned; there is some metallurgical evidence that for surface deposits considerably thinner than the present foils, a density 10 percent less than for bulk metal should be used.§§ For the foils used in this work which were several thousand atomic layers thick, there is less reason to expect a density uncertainty. To investigate this point, Warshaw estimated the amount of metal in his foils, whose thickness had been measured interferometrically, by quantitative chemical analysis, as follows.

(c) *Gravimetric chemical analysis.*—This could, of course, be used as a primary method of thickness determination, but Warshaw (Wa49a) used it to verify his use of bulk metal density in connection with the interferometric method for thickness. Foils which had been deposited on the glass slides for interferometric measurements were subdivided into accurately defined areas, which were then dissolved off in acid, and quantitatively analyzed by titrating the 8-hydroxy quiniline precipitate against standard bromate, according to well-known methods (Ko36). The accuracy of such a chemical determination was about ±1.5 percent; when used in connection with the interferometric thickness measurements, it indicated that the density of the evaporated foil was not more than 2 percent lower than the density of the bulk material.

The possibility that surface films may form over the

†† Type FDJ, manufactured by Wm. Ainsworth and Son, Inc., Denver, Colorado.

§§ L. Schultz, Institute for the Study of Metals, University of Chicago (private communication).

foils in the vacuum, increase the loss of energy, and thus introduce systematic errors, is always present. It will lead to values of the stopping power which are too high. Unfortunately, it is not always, or in fact, usually, possible to weigh the identical piece of foil which was introduced into the vacuum before and after the determination of ΔE. A run may be discarded as bad if the ΔE from a given foil appears to increase in magnitude with time in the vacuum, but this does not dispose of the possibility that the surface layers are laid down almost instantaneously upon introduction into the vacuum. It is known that heating the target before bombardment will greatly reduce the rate of accumulation of any deposit (Ha38, Br51, page 965), but heating of the thin foils in the vacuum was not attempted in the work of the Chicago group. In the work of Kahn (Ka53), the van de Graaff accelerator was evacuated with a mercury vapor diffusion pump, trapped with liquid nitrogen. The foil chamber and electrostatic analyzer were evacuated from a separated system with an organic oil (not a silicone) diffusion pump. A valve in the high-vacuum line between pump and foil was always closed except when the pump was trapped with liquid nitrogen. A series of measurements carried on for four days on the same foil showed no increase in ΔE, but the most that can really be said concerning the Chicago group experiments in this respect is that all precautions were taken to minimize the deposition outside of actually heating the foils.

2. *The Copenhagen Experiments*

The experiments in Copenhagen on the stopping power of solids for protons have been carried out by Madsen and Venkateswarlu (Ma48a, b), Huus and Madsen (Hu49), and Madsen (Ma53). The technique used by these investigators for the measurement of ΔE was quite different from that of the Chicago group. A van de Graaff generator was used as a proton source and a target material was selected which showed sharp resonances for gamma ray or neutron production. When a foil was interposed in the beam, it was necessary to increase the energy of the proton beam to excite the gamma rays or neutrons, and this energy increase gives the energy loss in the foil. Madsen found the following resonances to be useful for such measurements, one criterion being that the material show no other resonances in the immediate vicinity:

$F(p, \gamma)$	at 339 kev and at 660 kev;
$Al(p, \gamma)$	at 630, 986, and 1255 kev;
$Cl(p, \gamma)$	at 860 kev;
$Cl^{35}(p, n)$	at 1974 kev.

The neutrons or gamma rays were detected by standard counting techniques.

The foils were placed in a rotating holder which could either interpose them in the proton beam or leave it unhindered for the measurement of the initial energy.

Besides the foils, so-called "sandwich targets" were prepared and used. Madsen describes these in the following way:

> "On three or four discs of the supporting material (copper or or silver), a layer containing the energy indicator (fluorine, aluminum, or chlorine) was evaporated. One or two discs were removed from the evaporation chamber, while the stopping substance (Be, Al, Au, Ag, or Bi) was evaporated on the energy indicator layer. In this way, heating of the foil is avoided and a greater beam current can be applied. Moreover, a decrease in intensity of the radiation from the energy indicator, caused by scattering, is thus prevented."

Although the sandwich targets had certain advantages, a satisfactory absolute measurement of their thickness was not obtained, and the energy loss of such targets was always compared with that from a free foil of known thickness in order to obtain the target thickness. Having done this at a certain energy, the calibrated sandwich target could then be used for stopping power determinations at higher energy. For instance, with an aluminum indicating layer, the thickness of the sandwich foil could be found by comparison with a free foil at the 986-kev $Al(p, \gamma)$ resonance, and then the sandwich target used for measurements at the higher, 1255-kev resonance in aluminum.

In addition to measuring the stopping power of his foils, Madsen recorded the energy straggling of the beam caused by the randomness of the stopping process within the material. This resulted in an increase in the width of the resonance curve of the indicator when the foil was in the beam. Although the presence of energy straggling was obvious in the curves taken by the Chicago group, no record of it was kept.

3. *Experiments at Ohio State University*

Measurements of the stopping powers of metals and gases for protons in the low-energy range have been carried out at Ohio State University under the direction of J. N. Cooper (Ch53). The technique used was that of Madsen and Venkateswarlu (Ma48a, b) and the proton energies were in the region 450–1100 kev. Commercial foils of copper and nickel have been used, and the results indicate curves of dE/dx which run parallel to those of Kahn (Ka53), but are from 3 to 5 percent lower in dE/dx value for the same energy. Such a discrepancy is uncomfortably large, but not seriously outside the combination of internal consistency and systematic errors with which stopping power work is now being carried out. The use of commercial foils has been criticized by Warshaw (Wa49b), who found that the apparent stopping power for protons varied as much as 30 percent in foils of the same weight per unit area where a large area was taken for weighing purposes and the beam sent through a randomly selected small area in the larger one. Mention is made below of a technique used by the Ohio State group to investigate the consistency in thickness of their commercial foils. We may also note that the stopping power for protons measured by Wilcox from commercial gold leaf proved

to be approximately 15 percent low after evaporated gold foils had been prepared and used.

4. *Correction for Foils of Finite Thickness*

Since all foils used in dE/dx measurements are of finite thickness, there can, of course, be no sharp quantitative distinction between "thick" and "thin" foils. But it is of some use to make the rough distinction that a foil which, in a given experiment, absorbs more than 20 percent of the incident ion energy should be thought of as "thick," for that ion and energy. The prevailing practice is to measure the energy loss E_0-E_t, and to set the quotient $(E_0-E_t)/t=-(dE/dx)$, assigning the energy $\frac{1}{2}(E_0+E_t)\equiv E_{Av}$ as the energy to which the measurement of dE/dx pertains. If the variation of dE/dx with energy is rapid in the interval E_0-E_t, such a procedure is only approximate, and we will now inquire into the validity of the approximation. If an analytic expression is known or assumed for the variation of dE/dx with E, the correction can be calculated. The following rather general treatment of the problem is the suggestion of Harvey Casson.

Let it be known or assumed that

$$dE/dx=-1/f(E),$$

so that we have, on integrating from $x=0$ to $x=t$,

$$t=\int_{Et}^{E_0} f(E)dE.$$

The problem may now be stated: find an effective energy E_e (with $E_0>E_e>E_t$) such that

$$(E_0-E_t)/t\equiv\Delta E/t=-(dE/dx)_{Ee};$$

from this and the definition of $f(E)$,

$$f(E_e)=\frac{1}{\Delta E}\int_{E_t}^{E_0} f(E)dE.$$

Now let $E=E_0(1-\epsilon)$ and expand $f(E)$ near E_0, for small ϵ, in the form

$$f(E)=\sum_{n=1}^{\infty} A_n\epsilon^n.$$

If we substitute this expansion in both the right and left sides of the above integral, we get, on integrating,

$$\sum A_n\epsilon^n=\sum\frac{A_n}{n+1}\epsilon^n.$$

This can be put into the form of a series expansion of ϵ_e as a function of ΔE by successive differentiation with respect to ΔE and observing that $\epsilon_e=0$ for $\Delta E=0$. If one equates coefficients to a Taylor expansion of

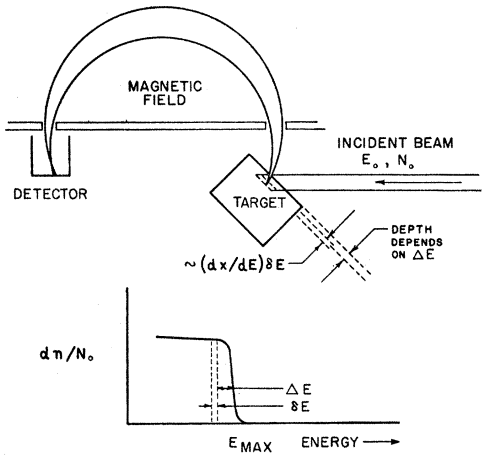

FIG. 6. Schematized spectrometer and spectrum for determination of dE/dx from scattering.

$\epsilon_e(\Delta E)$, one then gets

$$\epsilon_e=\frac{\Delta E}{E_0}\left(1+\frac{A_2}{6A_1}\left(\frac{\Delta E}{E_0}\right)+\cdots\right)$$

or, to second-order terms,

$$E_e=E_{Av}\left(1-\frac{A_2}{12A_1}\frac{\Delta E^2}{E_0E_{Av}}\right).$$

If we take $dE/dx=-(A/E)\log bE$, expansion of f and substitution of coefficients gives

$$E_e=E_{Av}\left(1-\frac{1}{24}\frac{(B+2)}{B(1-B)}\frac{\Delta E^2}{E_0E_{Av}}\right)\cdots, \qquad (13)$$

where

$$B=\log bE.$$

If, however $dE/dx\sim E^{-\frac{1}{2}}$ (as in Bohr's estimate for low-energy stopping in heavy elements),

$$E_e=E_{Av}\left(1+\frac{1}{48}\frac{\Delta E^2}{E_{Av}E_0}\right). \qquad (13')$$

In any case, the correction is clearly small.

5. *Stopping Power Determined by Intensity of Scattering and by Displacement of the Scattering Edge*

Wenzel and Whaling (We52) have used a technique for measuring the stopping power of solids which does not involve the preparation of a foil. The particles whose stopping power is to be measured are scattered from a thick target, and some of the scattered particles are accepted into a momentum (magnetic) or energy (electrostatic) analyzer. The counting rate for the scattered particles passing through the analyzer depends directly on the stopping power of the target material for the beam particles. Figure 6 illustrates the

essential features of the method. The scattered particles emerging from the target at angle θ to the primary beam will have a continuous energy spectrum because of stopping losses in the target, with an upper energy limit $E_{\max}$, where

$$E_{\max}=E_0\phi(m, M, \theta),$$

and

$$\phi(m, M, \theta)\lesssim 1, \tag{14}$$

because of momentum transfer to the target nuclei on scattering. The analyzer will transmit a narrow energy spread δE of scattered particles, and let us assume that the analyzer field is set so that the interval δE is located near an energy $E_{\max}-\Delta E$, where $\Delta E/E_{\max}$ is small, that is, near the upper energy limit of the continuum. More precisely, δE is the spread in energy accepted, from a point in the target, by the analyzer at a single field setting. This δE, multiplied by $(dE/dx)^{-1}$ and by a suitable geometric factor depending on the inclinations of the incident and scattered ray to the normal to the target face, will determine the thickness of a layer (in general, buried beneath the target surface) in which the measured scattering originated.

In order to obtain reliable dE/dx values, cases must be chosen in which the scattering cross section is known, and this usually means that beam particle and target must be chosen such that one can be sure that pure Rutherford scattering, uncomplicated by nuclear force fields, is taking place. The differential scattering cross section is then (Da14)

$$\frac{d\sigma}{d\omega}=\left(\frac{zZe^2}{mv^2}\right)^2 \operatorname{cosec}^3\theta\frac{[\cot\theta\pm(\operatorname{cosec}^2\theta-(m/M)^2)^{\frac{1}{2}}]^2}{(\operatorname{cosec}^2\theta-(m/M)^2)^{\frac{1}{2}}}. \tag{15}$$

- $d\sigma$ is the differential cross section per target nucleus for scattering into differential solid angle $d\omega$ at scattering angle θ in the laboratory system.
- m; M are the masses of the projectile and target nuclei, respectively.
- z; Z are the atomic numbers of beam and target nuclei.
- v is the speed of the projectile nucleus in the laboratory system.
- θ is the scattering angle in the laboratory.

Both experiment and detailed calculation show that the continuous energy spectrum is quite flat near its upper energy limit at $E_{\max}$, and if the analyzer is set so that $\Delta E/E_{\max}\sim 1$ percent, the counting rate is independent of ΔE.

The solid angle of acceptance of the analyzer Ω, in steradians, can be calculated from the geometry of the instrument, or may be found experimentally by quantitative scattering experiments in which the pertinent dE/dx values are known from foil measurements.

It is not advisable to give a general formula for dE/dx from this method, where magnetic or electrostatic analysis, in different target geometries, may be used. A simple case is an electrostatic analysis with an instrument aperture of such a shape that all the scattered particles which are accepted leave essentially at the same angle to the target face normal. (Such is not the case, for instance, in the spherical analyzer of Allison and Casson (Al53).) Also, for simplicity, we consider a target geometry such that incident and scattered rays make the same angle with the normal to the target face. Then we have

$$\delta n/N_0=N_T(dE/dx)^{-1}\cdot(d\sigma/d\omega)\cdot\delta E\cdot\Omega, \tag{16}$$

where

- $\delta n/N_0$ is the fraction of the incident beam particles detected per second as focused, scattered particles;
- N_T is the number of target nuclei per cm^3;
- δE is the energy interval, in electron-kilovolts, accepted by the analyzer from a point in the target, at a given field setting. δE is calculable from the orbit characteristics and object aperture dimensions of the instrument;
- dE/dx is the stopping power in kilovolts per cm of the target material for beam particles of energy $(E_{\max}-\Delta E)$;
- $d\sigma/d\omega$ is the differential scattering cross section, Eq. (15);
- Ω is the solid angle or acceptance of the analyzer in steradians.

Variants of this equation, suitable to their own instruments, have been given by various experimenters (We52, Sn50, Br51).

Wenzel and Whaling (We52) have also used a method for dE/dx in solids which depends on the displacement of the scattering edge at $E_{\max}$ (Fig. 6) in case a layer of material of Z different from that of the thick target forms on its surface. This effect is often seen in scattering experiments in which a layer of carbon is forming over the target surface because of imperfect vacuum conditions. In their experiments D_2O ice was formed on the face of a copper target cooled with liquid nitrogen. The Z's in the D_2O are so low that the Coulomb scattering is small compared to that of the copper substrate, but also, and of more importance, there is the fact that the relatively large momentum and energy transfers to the D and O nuclei throw the energies of the particles scattered from them well below $E_{\max}$ for the substrate. Thus, after energy or momentum analysis, the copper scattering edge is free of contamination from D or O scattering, as from the bare target. If one can be sure that layers of frozen material are formed which retain their same thickness during the time necessary for several experimental runs, the shifts of the copper scattering edge to lower energies are directly interpretable as relative values of dE/dx for the surface layer at different beam energies.

6. Discussion and Tables

With the exception of the results on beryllium and mica, all the Copenhagen data are based on dE/dx values obtained from commercial (rolled or beaten) metal foils. We will first discuss the data on beryllium and mica foils, which were specially prepared in the laboratory for the measurements.

Data Obtained from Foils Prepared in the Laboratory

Beryllium.—The data of Madsen, *et al.* shown in Table III-1 were taken on weighed, evaporated foils. Hence, the technique of foil preparation was similar to that of the Chicago group. Furthermore, there is in general good agreement between Kahn and Madsen where their data overlap. In the region 500 to 1150 kev the largest discrepancy is at 1133 kev where Madsen's value of 203 lies 5 percent above Kahn's curve of dE/dx in kev$\times$cm^2/mg *vs* energy. At 455 kev Madsen reports a dE/dx value of 377 kev$\times$cm^2/mg from a Be foil in which the loss of energy was 230 kev or 40.3 percent of the incident proton energy. At 436 kev, Kahn's value for dE/dx is 347 in these units. Madsen's results show that the energy straggling for this determination, compared to the energy, was very much larger than for his other determinations on beryllium, and we have not attached sufficient reliability to it to modify the Kahn-Warshaw curve in its vicinity.

Unfortunately, in the case of beryllium, the absolute error in Kahn's data may be the greatest of all his experiments because of his difficulties in obtaining a piece of foil large enough for a reliable weight determination. Kahn states that the error in absolute value may possibly be 15 percent. In the region above 1150 kev, near 1276 kev, the dE/dx value of Madsen is 11 percent greater than that of Kahn, and this has caused us to raise the stopping power values in this region close to the results reported by Madsen. The combined data of Madsen, Kahn, and Warshaw has been used to construct the beryllium curve of Fig. 7 and the beryllium data in Table III-7.

Mica.—Mica, of course, is a substance of possibly variable composition; the variety used by Kahn is properly known as muscovite. Foil thicknesses were measured gravimetrically in both researches, but Madsen investigated his foils for homogeneity using an interferometric method due to Tolansky (To45, To47). The stopping power values obtained by Madsen in the region 400–1100 kev lie slightly above a smooth curve through Kahn's points, the largest discrepancy being 6.7 percent for the values of 1072 kev. Madsen's point at 1279 kev lies exactly coincident with Kahn's value of 143 kev$\times$cm^2/mg at 1245 kev, and we interpolate to Madsen's point at 2000 kev with considerable confidence. Values from Kahn and Madsen appear in Fig. 8 and in Table III-7.

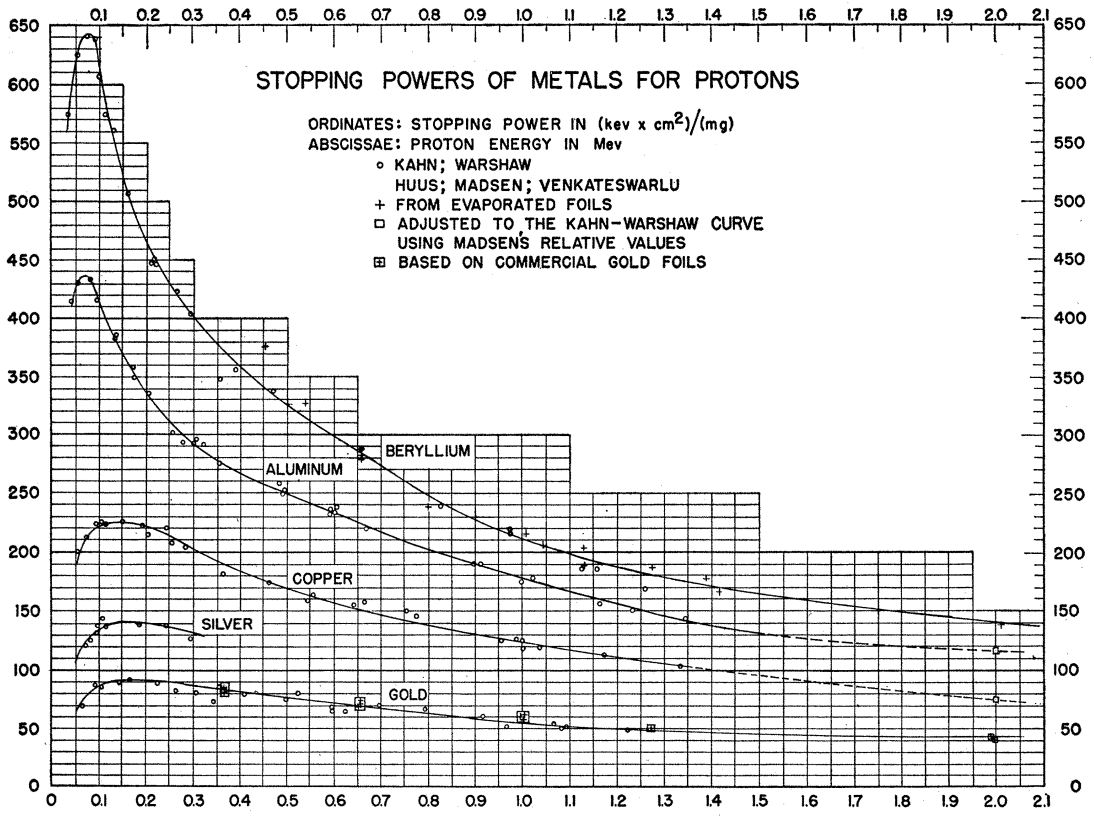

Fig. 7. Combined equipmental data for dE/dx in the 0-2-Mev proton range.

Data Obtained from Commercial Foils

The Copenhagen data on Al, Cu, Ag, and Au all depend, in their absolute value, on stopping powers measured in commercial foils. In some cases Madsen used "sandwich" foils in which a layer of the stopping substance was evaporated over a layer of detecting material on a solid mounting. However, the thickness of these "sandwich" foils was always determined by comparing the energy loss (or sometimes the straggling) with that produced by a weighed commercial foil.

The Chicago group has had trouble with commercial foils in the past. Warshaw (Wa49b), who investigated the reliability of commercial aluminum foils for dE/dx measurements, reports as follows:

". . . four rolled and two evaporated foils were used to determine the stopping power in aluminum. The surface densities of the commercial foils were determined by accurately weighing known areas (about 50 cm²). The resulting curves from the commercial foils deviated as much as 30 percent from the average curve. On the other hand, data from both of the evaporated foils fell on the same curve (within the standard deviation of all points), and furthermore, within 8 percent of the average of the curves obtained from the commercial foils."

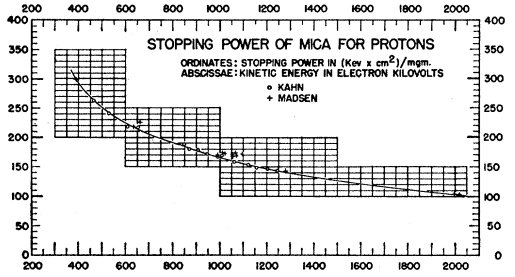

FIG. 8. Data of Kahn and Madsen on stopping power of mica.

In fact, Madsen's dE/dx values from commercial aluminum and copper foils fall seriously off Kahn's curves, typical discrepancies being that Madsen is 11.4 percent low at 689 kev in aluminum, and 17 percent low at the same energy in copper. In view of our experiences with rolled foils, we have disregarded the absolute values of the Copenhagen results on aluminum and copper. The relative values at different energies, however, are much more reliable, and we have used Madsen's relative dE/dx values at 1993 and 1022 kev in aluminum (ratio 0.643), and at 2002 and 1012 kev in copper (ratio 0.623) to establish a point for these stopping powers at the upper limit of our energy range. By taking the absolute values at the lower voltages from Kahn's curve, we find a dE/dx value of 112 at 1993 kev for aluminum, and 75.4 at 2002 kev for copper. We have used these adjusted results of Madsen's work to continue Kahn's curve to the upper energy limit.

Madsen's dE/dx values for gold, based on commercial foils, and in some cases adjusted to gold from measurements on bismuth, agree well with Kahn's data on evaporated foils, which, in turn, join on smoothly to Warshaw's gold values. The agreement may possibly be fortuitous, because in the Chicago laboratory the stopping power for protons obtained by Wilcox (Wi48) in a commercial gold foil was 14 percent lower than Warshaw and Kahn's evaporated foil values, and Wilcox was led to incorrect (Ha49) conclusions regarding deuteron *vs* proton stopping powers using different commercial foils of gold. The extended region of agreement in gold between the Copenhagen and Chicago results has led us to decrease our estimate of the reliability of Warshaw's three highest energy points on gold, and to draw the dE/dx curve above them. We have extended the curve to 2000 kev with considerable confidence.

Kahn did not take data on silver, and unfortunately the data obtained by Madsen on commercial foils do not overlap those of Warshaw. In view of the fact that

TABLE III-1. Stopping power of beryllium metal for protons. (C. B. Madsen, *et al.* from evaporated foil.)

Energy loss in foil (kev)	Mean proton energy in foil (kev)	dE/dx kev×cm²/mg
230	455	377
73	540	329
62	661	279
64	662	288
69	665	282
53	798	239
48	1010	216
48	1010	216
53	1013	216
126	1049	207
42	1133	189
45	1135	203
42	1276	188
108	1310	177
39.5	1392	178
101	1422	166
85	2016	139

TABLE III-2. Stopping power of aluminum metal for protons. (C. B. Madsen, *et al.*, from commercial Al foil.) (These values run about 11 percent below those recommended in Table III-7.)

Energy loss in foil (kev)	Mean proton energy in foil (kev)	dE/dx kev×cm²/mg
58	368	252
95	387	250
42	681	182
70	695	185
38.5	1005	167
59.5	1016	157
72	1020	150
82	1025	164
31	1270	135
53	1281	139
23	1986	100
37	1993	98
37	1993	100[a]
39	1994	105[a]

[a] "Sandwich" target calibrated from commercial foil.

TABLE III-3. Stopping power of copper metal for protons. (C. B. Madsen, *et al.*, from commercial copper foil.) (These data run 14–20 percent below those recommended in Table III-7.)

Energy loss in foil (kev)	Mean proton energy in foil (kev)	dE/dx kev $\times$cm²/mg
73	376	149
90	384	155
60	690	122
70	695	121
53.5	1012	109
53.0	1012	106
56.5	1014	98
46	1278	94
51	1281	88
35	1991	72
46	1997	79
41.4	1994	70
54	2001	64[a]
56	2002	67[a]

[a] "Sandwich" target, Cl indicator, calibrated at 860 kev.

Madsen's values of dE/dx from commercial foils of Al and Cu do not lie on the Kahn-Warshaw curves for those elements, we have not used his silver values to extend Warshaw's silver points to higher energies, but have tabulated them separately.

Tables III-1 to III-5 contain the experimental results

TABLE III-4. Stopping power of silver metal for protons. (C. B. Madsen, *et al.*, based on commercial silver foil.) (This is the only available experimental data on Ag above 350 kev.)

Energy loss in foil (kev)	Mean proton energy in foil (kev)	dE/dx kev $\times$cm²/mg
59	369	137[a]
60	370	143
60	370	143
51	365	142
84	381	142
209	445	138
22.8	641	101[b]
22.6	641	96[b]
32.5	646	114[b]
36	678	100
44	683	100
64	692	108
47.5	880	93[d]
33	1003	91
34.7	1004	82
38.5	1005	80
40	1006	82
53	1012	90
130	1051	86
15.9	1263	71[b]
15.9	1263	71[b]
29.6	1270	68[b]
29	1989	59
47.5	1998	59[c]
90	2019	60

[a] "Sandwich" target, fluorine indicator, calibrated at 660 kev.
[b] "Sandwich" target, aluminum indicator, calibrated at 986 kev.
[c] "Sandwich" target, chlorine indicator, calibrated at 860 kev.
[d] "Sandwich" target, chlorine indicator, calibrated at 1974 kev.

TABLE III-5. Stopping power of gold metal for protons. (C. B. Madsen, *et al.*, from commercial gold foils.)

Energy loss in foil (kev)	Mean proton energy in foil (kev)	dE/dx kev $\times$cm²/mg
38.5	359	85
42	360	81
44	366	82[a]
41.9	651	71[b]
42.9	652	72[b]
49.4	655	76[b]
27	999	60
30	1000	58
31	1001	61
49.5	1009	59
29.6	1270	50[b]
29	1988	43[c]
28.7	1988	43[c]
34	1991	41

[a] Bi "sandwich" target; fluorine indicator, calibrated at 660 kev.
[b] Bi "sandwich" target; aluminum indicator, calibrated at 986 kev.
[c] Bi "sandwich" target, chlorine indicator, calibrated at 860 kev.

on dE/dx at present available to us from the Copenhagen group.

At Ohio State University (Ch53) measurements of stopping powers of metal foils for protons have been carried out using the shift-in-resonance technique of Madsen. The foils used were those commercially available from the Chromium Corporation of America, and varied in surface density from 0.67 to 2 mg/cm². The thickness variation from point to point on the thin foils was tested by allowing alpha particles from polonium to traverse a small area of the foil and observing the variation in range as the point of transmission was varied over the foil. The conclusion was reached that if the average thickness of the foils, as

TABLE III-6. Data of Chilton, Cooper, and Harris (see reference Ch53) on the stopping power of nickel and of copper for protons.

Proton energy (kev)	Nickel kev $\times$cm² / mg	Prob. error %	Proton energy (kev)	Copper kev $\times$cm² / mg	Prob. error %
527	172.3	1.5	446	171.1	
704	148.7	2.0	532	160.0	
718	150.1	3.0	603	152.0	1.5
739	142.8	2.0	713	141.6	1.5
741	141.7	2.0	755	138.7	2.0
755	145.6	1.5	812	133.2	1.5
757	146.5	1.5	949	121.5	2.0
915	128.4	3.0	996	116.0	1.5
935	125.8	2.0	1006	113.3	2.0
941	133.7	2.0	1050	114.5	2.0
949	128.5	2.0			
951	128.5	2.0			
977	129.1	3.0			
1000	127.5	2.0			
1007	122.0	2.0			
1046	120.6	2.5			
1047	122.1	2.5			
1057	120.9	2.0			

determined by weighing known areas, was used, the variation in thickness would not account for more than a 1 percent error in dE/dx.

The results of the investigations on Ni and Cu are given in Table III-6. The measured dE/dx values lie from 4 to 5 percent below those on the Kahn-Warshaw curve (in the case of copper) as shown in Fig. 7 and Table III-7.

7. *Stopping Power of Solid D_2O for Protons and Deuterons*

Stimulated by the interest in the cross sections of the (d, d) and (t, d) reactions, Wenzel and Whaling (We52) have measured the stopping power of D_2O ice for protons and deuterons by the methods previously described. The results, stated in terms of the molecular stopping power in electronvolts per molecule per cm^2 are believed to contain a probable error of 4 percent, and are given in Table III-8.

It was found by experiment, as indicated by theory, that the stopping powers for protons and deuterons of the same speed are equal. Thus, the table may be used for the stopping power of D_2O ice for deuterons, by assuming that the value given for each proton energy applies to deuterons of twice that energy.

TABLE III-7. The proton energy loss as a function of energy.

Proton energy (kev)	dE/dx (kev×cm^2/mg) Be	Mica (Muscovite)	Al	Cu	Au
25	546				
50	617		422	185	61
75	640		439	212	77
100	615		416	221	87
150	521		366	225	90
200	468		334	222	91
250	433		314	212	90
300	405		293	202	86
350	381	312	279	190	84
400	360	286	268	183	81
450	342	266	258	175	79
500	325	250	250	169	76
550	311	236	241	162	74
600	298	224	233	156	72
650	284	214	224	151	70
700	272	204	217	146	68
750	266	196	210	141	66
800	251	189	202	138	64
850	241	182	196	133	62
900	232	176	190	129	60
950	223	171	183	127	58
1000	215	165	177	124	56
1050	206	160	171	120	54
1100	198	154	165	117	52
1150	192	150	159	113	51
1200	188	146	154	110	49
1250	182	143	148	108	48
1300	178	139	143	105	47
1350	175	136	139	102	46
1400	171	133	135	100	45
1500	164	127	127	96	44
1600	158	122	123	91	42
1700	152	117	120	88	42
1800	148	112	117	83	42
1900	144	108	115	79	42
2000	139	102	112	75	42

TABLE III-7A. Conversion factors for expressing stopping powers of metals in various units.

Given units	Units desired: kev×cm^2/mg	ev×cm^2/atom	erg/cm	kev/cm
kev×cm^2/mg	Au 1	327×10^{-18}	309×10^{-7}	193×10^{2}
	Ag 1	179	168	105
	Cu 1	106	143	89.3
	Al 1	44.8	43.2	27.0
	Be 1	15.0	29.6	18.5
ev×cm^2/atom	3.06×10^{15}	Au 1	9.46×10^{10}	5.91×10^{19}
	5.59	Ag 1	9.39	5.86
	9.43	Cu 1	13.57	8.47
	22.2	Al 1	9.66	6.03
	66.7	Be 1	19.87	12.35
erg/cm	3.24×10^{4}	1.057×10^{-11}	Au 1	6.243×10^{8}
	5.95	1.065	Ag 1	6.243
	6.99	0.737	Cu 1	6.243
	23.2	1.035	Al 1	6.243
	33.8	0.503	Be 1	6.243
kev/cm	5.18×10^{-5}	1.692×10^{-18}	1.602×10^{-9}	Au 1
	9.524	1.706	1.602	Ag 1
	11.20	1.181	1.602	Cu 1
	37.0	1.658	1.602	Al 1
	54.0	0.809	1.602	Be 1

8. *Recommended Low-Energy Stopping Power Values for Protons in Metals and Mica; Formulas for Interpolation and Extrapolation*

Figures 7 and 8 and the numerical values in Table III-7 present a set of dE/dx values for protons in metals and mica, obtained by averaging weighted values from the experiments of Warshaw (Wa49b), Kahn (Ka53), and the values communicated to us from Copenhagen by Madsen. The data of Chilton, Cooper, and Harris (Ch53), given in Table III-6, were received at too late a date to be included in the averaging process. In copper, where there are serious discrepancies between the results of Kahn and Madsen, the data of Chilton, *et al.* lie slightly below, but close to, Kahn's results. It seems reasonable to suppose that the recommended values in the figure and the table are correct to within 5 percent.

Light elements.—For the light elements, the fastest moving electron may still have lower speed than that of the moving ion for relatively low energy (see Sec. II), and therefore it is expected that the Bethe-Bloch equation for stopping power, with values of I empirically fit, can be used at these low energies. Further, the constancy of these values of I can be used as a test of the validity, and therefore usefulness, of the theory.

Beryllium.—Table III-9 shows considerable variations in the value of I for Be in the region 1000–2000 kev, when I is calculated from experimental values. However, the fact that I is in the argument of the

TABLE III-8. Molecular stopping power of D_2O ice for protons.[a]

Proton energy (kev)	Stopping power in ev×cm²/molecule
18	15.6×10^{-15}
20	17.4
30	20.4
40	22.6
50	23.5
60	24.0
70	24.1
80	24.0
100	23.7
125	23.0
200	20.1
300	16.0
400	13.3
500	11.6
540	11.2

[a] See reference We52.

logarithm makes it quite sensitive to fluctuations in the experimental value of dE/dx. Madsen and Venkateswarlu (Ma48a) found that $I=64$ ev gave the best fit to their data between 500- and 1500-kev proton energy. A value of $I=57$ ev will fit the curve of Fig. 7 to within 3 percent in the range 1600–2000 kev and can be recommended for cautious interpolation and extrapolation in and beyond this region. Using this value for I, we obtain the following formula for protons in beryllium, with E in kev,

$$\frac{dE}{dx}(\text{kev}\times\text{cm}^2/\text{mg}) = -\frac{6.385\times10^4}{E}\log_e(3.818\times10^{-2}E) + \frac{1.597\times10^4}{E}C_K, \quad E>1600 \text{ kev}, \quad (17)$$

with C_K values from TableII–1. The K-correction term affects dE/dx by 4 percent at 2000 kev, and its effect decreases above this proton energy.

Aron (Ar51) has computed stopping powers for protons in beryllium from 1 Mev to 10^4 Mev using $I=59$ ev [and, of course, for the higher energies, the relativistic Eq. (3)]. The value of I used by Aron was consistent with that found in the experimental work of Mather and Segrè (Ma51) on the range-energy relation for protons in beryllium at 340 Mev, and we see that the value of I appears to be essentially the same at 1600 kev and 340 Mev. Aron's calculated numerical values of dE/dx for a given I are slightly different (2.3 percent higher at 2 Mev) than those calculated in this report (see note in Sec. II).

As previously mentioned in this report, the experimental errors in the stopping experiments on beryllium are unfortunately large, and better data might reveal a more constant value of I than is exhibited in Table III-9.

Aluminum.—If one uses a value of $I=162$ ev for aluminum, the nonrelativistic Bethe equation for dE/dx for protons in the metal becomes (E in kev)

$$\frac{dE}{dx}(\text{kev}\times\text{cm}^2/\text{mg}) = -\frac{6.944\times10^4}{E}\log_e(1.344\times10^{-2}E) + \frac{5.34\times10^3}{E}C_K. \quad (18)$$

This expression, with values of C_K from Table II-1 will fit the numerical values of the data at 1400 and 2000 kev within 5 percent. Bloembergen and van Heerden (Bl51) found $I=159$ for 70-Mev protons in aluminum, and Mather and Segrè (Ma51) found $I=148$ at 340 Mev. The value indicated above as fitting the data around 2000 kev is nearer to the value found for 70-Mev protons (see Sec. IV).

Heavier elements.—In the case of the heavier elements, nickel, copper, silver, and gold, the simple stopping power equation cannot be used in the energy region of this section, and thus a theoretical guide for interpolation and extrapolation is not available.

It may be noted that there is a large discrepancy between the dE/dx values of Pb for 1- and 2-Mev protons as calculated by Aron (Ar51) and as inferred from measurements on the nearby element, gold. Assuming that the stopping power in ev×cm²/atom varies as $Z^{\frac{1}{3}}$, and using the observed values 56 and 42 in kev ×cm²/mg for gold at 1000 and 2000 kev, one finds the stopping power in these units for Pb should be 54 and 40 in kev×cm²/mg at 1 and 2 Mev, respectively. Aron's calculated values are 71 and 51.

9. *Stopping Power of Gold for Helium Ions*

There is need for more work by experimental physicists on the stopping power of metals and solids for helium ions. At high energies, above 2 Mev, where the moving particle is always He^{++}, the atomic stopping powers should be calculable from Eq. (3), with the I appropriate to protons. There is, however, no theory at present capable of including the lower-energy region where the forms He^0, He^+ also appear in the moving beam.

TABLE III-9. I from experimental data: beryllium.

Proton energy (kev)	dE/dx (observed)	$I_{calc.}$ (ev)
1000	215	64
1200	185	70
1400	166	71
2000	140	50

The only direct measurements of stopping power for helium ions in solids in our energy region are those of Wilcox (Wi48), and these unfortunately are vitiated in that the commercial gold foils he used evidently led to errors in related experiments (Wa49b, Ha49). Fortunately, however, Wilcox published values of the loss of energy of protons in these same gold foils, and through the recent reliable data for the stopping of protons in gold we are able to deduce what the effective thickness of his gold foils was. In this way the data of Fig. 9 were computed; Wilcox's original dE/dx values have been increased about 14 percent. Because of the uncertainty of the correction and the evidence of some internal errors of measurement from the spread of his points at higher energies where the disintegration alpha particles from $Be^9(p, \alpha)Li^6$ were used, there may well be 15 percent error in the results summarized in the figure.

B. The Stopping Powers of Gases for Various Ions

The first direct measurement of the stopping powers of gases for ions of energies within the range (20–2000 kev) of this report seems to have been made by Crenshaw (Cr42). The beam of protons or deuterons, of kinetic energies in the range 60–340 kev, was passed through a differentially pumped gas absorption cell, and the effect of introduction of the gas in lowering the energy of the transmitted beam was determined by magnetic analysis of the emergent particles. This early work has been repeated and extended by several investigators with greater accuracy than in the original, and Crenshaw's data will not be included here.

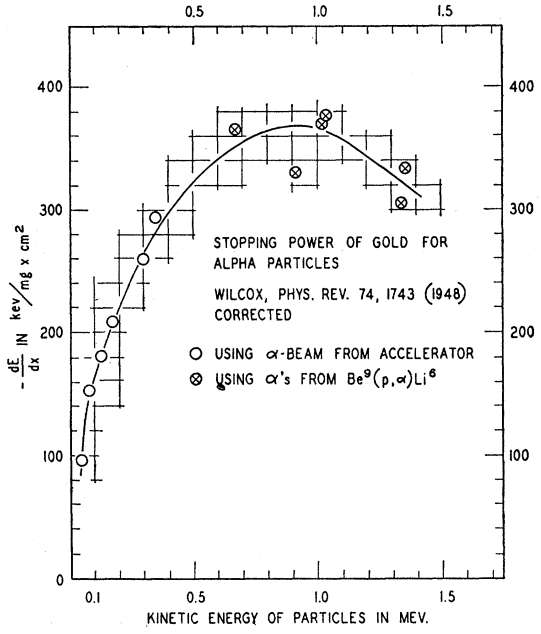

FIG. 9. The stopping power of gold for Alpha particles; corrected (see text, Sec. IIIA-1) from reference Wi48.

As discussed above, the range, as a quantitative measure of energy, loses much of its significance in the energy region under consideration. Evans, Stier, and Barnett (Ev53) have shown that if ions of He^+, N^+, Ne^+, and A^+ in the energy region 20 to 250 kev are admitted to various stopping gases, the range which is measured is a function of the geometry, and, if an ionization chamber of too small an aperture is used, the result in gm/cm² may appear to have a pressure dependence. We shall therefore emphasize in this report what can be learned about dE/dx itself, although, as we shall show, the present measurements give only the energy loss resulting from electronic impacts, whereas the losses due to atomic impacts in which large exchanges of energy and momentum occur, become increasingly important as the mass of the moving particles increases.

1. Methods

(a) *Methods used by the Chicago group.*—Figure 10 indicates schematically the technique used by Weyl (We53). The gases H_2, D_2, He, N_2, and Ne were at

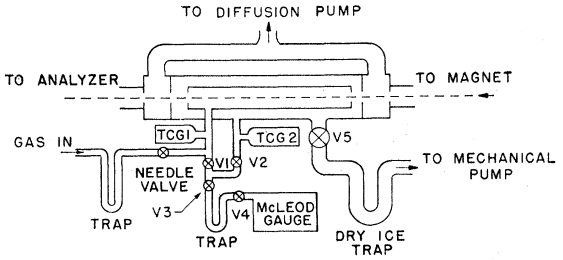

FIG. 10. Schematic of the gas absorption cell and associated equipment used by Weyl (see reference We53) for measurement of dE/dx in gases.

separate times fed into the low voltage arc of the Cockcroft-Walton accelerator, or "kevatron," for short. The accelerated ion beams were magnetically analyzed and the singly charged components H^+, H_2^+, D^+, He^+, N^+, or Ne^+ were directed toward a gas absorption cell which the beam then traversed. After passing through the gas cell, which could either be evacuated or filled with the gas whose stopping power was to be measured, the energy of the emergent beam was measured by electrostatic deflection in a 90° cylindrical analyzer (Al38).

The gas absorption cell consisted of a thin-walled cylinder 2.54 cm in internal diameter and 76.53 cm long, with holes in its ends 0.038 cm in diameter so that the ion beam could enter, traverse it longitudinally, and leave. The cell was enclosed in a larger tube 5.40 cm in outside diameter, and compartments at both ends of the cell were designed so that the pressure could be reduced in stages from approximately 0.5 mm in the cell to less than 10^{-5} mm Hg in the kevatron itself, and in the electrostatic analyzer. Thus, the only matter traversed by the ion beam from the low voltage arc

to the ZnS scintillator at the object focus of the cylindrical electrostatic analyzer was the gas whose stopping power was being determined. The pressure of the gas in the cell was measured by a sensitive McLeod gauge.

Weyl adopted a simple procedure which made the energy analysis of the beam after traversal of the gas cell independent of slight fluctuations in beam intensity. The 0.038-cm diameter entrance aperture to the absorption cell was so small that fluctuations of intensity within the focal spot of the beam affected the current through the cell. The outer plate of the cylindrical electrostatic analyzer, which would normally be grounded, was connected to a 60-cycle ac supply. The phase of this biasing ac could be shifted, and the impressed wave had an amplitude of 250-volts rms symmetrically above and below ground potential. Thus the ion beam leaving the analyzer was kept in 60-cycle oscillatory motion across the exit slit in front of the ZnS scintillator.

The output of the photomultiplier (see Fig. 4), which was activated by the light from the ZnS, was connected

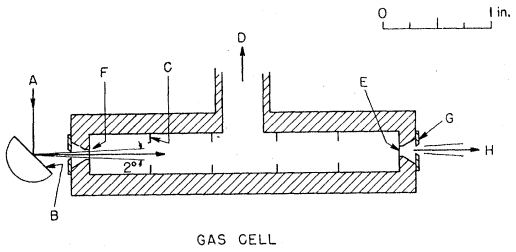

FIG. 11. Gas cell for dE/dx measurements as used by investigators at the California Institute of Technology (see reference Du52). *A*. Monoenergetic proton beam. *B*. Target (gold plated on copper). *C*. Baffles to prevent scattering from the walls. *D*. To manometer and gas handling equipment. *E*, *F*. Aluminum foil windows. *G*. Limiting aperture, 0.131-cm diameter.

to the vertical deflection plates of a cathode ray oscilloscope, and the horizontal sweep of the scope was driven by the biasing ac. By shifting the phase of the ac with respect to the phase of the 60-cycle ac on which the kevatron was operated, an oscilloscope trace with a single extremum could be produced. (More complicated curves resulted if the sweep was in arbitrary phase relationship with the ripple in the kevatron high voltage.) Fluctuations in beam intensity moved this extremum vertically, but only its horizontal location was needed to measure the beam energy by electrostatic deflection. The energy loss in the gas was determined by first adjusting the phase of the detector voltage so that a single peak appeared on the oscilloscope screen at a given (marked) abscissa, with no gas in the cell; the analyzer voltage for this condition then gave the initial energy. As gas was admitted to the cell, the peak moved horizontally and the shift in analyzer voltage required to bring the peak back to its original condition was taken as the energy loss. By using the analyzer constant (19.77 kev/kv) and correcting the

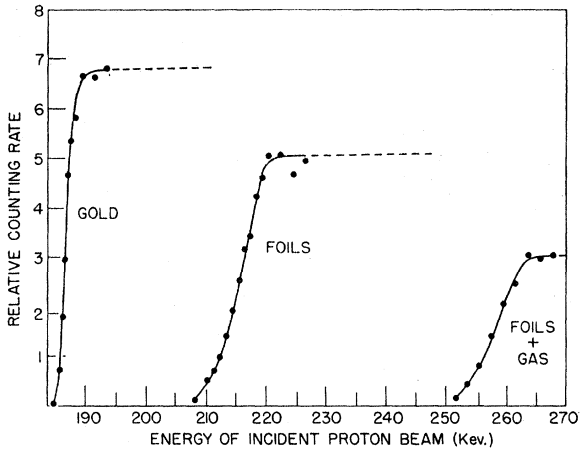

FIG. 12. Gas stopping power measurement by the California Institute of Technology group. "Gold": energy analysis of scattered protons from a gold target, see Fig. 11. "Foils": same spectrum degraded in energy by passage through foil windows. "Foils plus gas": additional energy loss when gas is introduced to the chamber.

McLeod gauge reading to 0°C, the stopping power was calculated.

(b) *Methods used at California Institute of Technology.*—Recently a group of investigators (Du52) at Pasadena have made measurements on the stopping power of a large number of gases for protons. The energy region covered was 30–600 kev. The gases were contained in an absorption tube 7.3 cm long, the entrance and exit ports being closed with aluminum foils each 4.5×10^{-2} mg/cm^2 in thickness (Fig. 11). The protons which were measured were scattered from a gold layer backed by copper, and the shift of the high-energy edge (Fig. 12) produced by admitting gas to the cell, through which the scattered beam passed, indicated the stopping power. A correction must be made because the gas has lowered the energy of the protons striking the second aluminum foil, and hence its stopping power has been changed (see Table III-7). The energy of the scattered beam which emerged from the absorption cell was determined in a magnetic momentum analyzer.

(c) *Method used at Los Alamos.*—Phillips (Ph53) has measured the stopping power of various gases for protons in the energy range 10–80 kev. The gases were contained in an absorption cell (see Fig. 13) by the use of

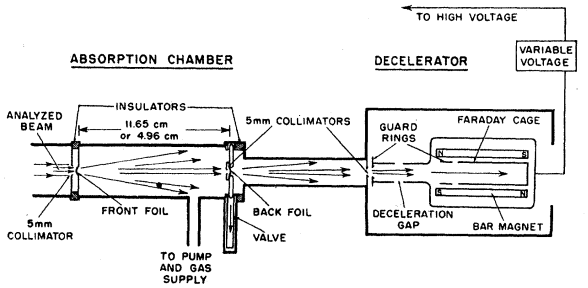

FIG. 13. Gas absorption cell and proton deceleration chamber used by J. A. Phillips (see reference Ph53).

SiO foils (Sa52) over the entrance and exit holes. These foils caused an energy loss of from 5 to 10 kev in the proton beam. For gases and energies where the energy loss in the cell was large at reasonable pressures, the chamber could be shortened to 4.86 cm in length; otherwise a length of 11.65 cm was used. The beam passed through 3 circular apertures 0.5 cm in diameter, two at the entrance and exit of the absorption cell, and one in front of the energy analyzing device.

The foil at the exit port of the absorption cell was mounted on a sliding valve so that it could be completely retracted from the line of motion of the beam, allowing a measurement of the loss in energy in the entrance foil alone. An investigation was made of the bowing out of the foils when gas was admitted to the cell, and it was found that the effect added 0.26 ± 0.03 cm to the length of the cell as defined by the planes of the window-supporting frames.

TABLE III-10. Stopping powers of the noble gases for protons in the energy range 20–1000 kev. Atomic stopping powers in $(\text{ev}\times\text{cm}^2/\text{atom})\times10^{15}$.

Proton energy (kev)	Reference	He	Ne	A	Kr	Xe
20	Ph53	4.83	···	23.3	26.0	···
30	Ph53	5.77	···	27.2	30.0	···
40	Ph53	6.51	···	30.0	33.4	···
40	Du52	6.67	10.6	31.4	35.6	50.0
40	We53	···	···	32	···	···
50	Ph53	7.07	···	31.4	35.5	···
50	Du52	6.97	11.9	33.4	38.3	52.6
50	We53	···	···	33	···	···
60	Ph53	7.26	···	31.6	36.6	···
60	Du52	7.22	12.8	34.3	39.8	53.5
60	We53	···	···	33	···	···
70	Ph53	7.33	···	30.7	36.9	···
70	Du52	7.33	13.45	34.4	40.5	53.5
70	We53	···	···	33	···	···
80	Ph53	7.41	···	29.2	37.2	···
80	Du52	7.37	13.95	34.1	40.5	53.2
80	We53	···	···	33	···	···
90	Du52	7.37	14.3	33.5	40.3	52.0
90	We53	···	···	32	···	···
100	Du52	7.30	14.6	32.6	39.8	50.6
100	We53	···	···	31.5	···	···
150	Du52	6.37	14.6	28.2	35.0	45.2
150	We53	···	···	29	···	···
190	We53	5.4	···	···	···	···
200	Du52	5.55	14.10	24.5	30.7	41.8
200	We53	···	···	25.5	···	···
250	Du52	4.91	13.20	21.6	27.4	38.6
250	We53	···	···	22	···	···
290	We53	4.4	···	···	···	···
300	Du52	4.41	12.34	19.5	25.1	35.8
300	We53	···	···	19.7	···	···
350	Du52	4.01	11.50	17.9	23.3	33.4
350	We53	···	···	18	···	···
360	We53	3.7	···	···	···	···
400	Du52	3.69	10.75	16.6	22.0	31.4
400	We53	···	···	16.5	···	···
420	Ch53	···	···	···	22.65	···
421	Ch53	···	···	14.87	···	···
422	Ch53	···	10.37	···	···	···
424	Ch53	···	9.70	···	···	···
437	Ch53	···	···	···	···	26.3
441	Ch53	···	···	···	···	26.4
450	Du52	3.42	10.15	15.55	20.9	29.8
476	Ch53	···	···	14.81	···	···
500	Du52	3.18	9.58	14.7	19.9	28.6
516	Ch53	···	···	···	20.75	···
517	Ch53	···	9.38	···	···	···
519	Ch53	···	8.91	14.28	···	···
527	Ch53	···	···	···	21.30	···
536	Ch53	···	···	···	···	24.1
538	Cu53	···	···	···	···	25.1
550	Du52	2.99	9.09	13.9	19.1	27.4
567	Ch53	···	···	13.71	···	···
600	Du52	2.81	8.65	13.3	18.4	26.4
662	Ch53	···	···	11.67	···	···
665	Ch53	···	···	···	18.07	···
668	Ch53	···	7.88	···	···	···
675	Ch53	···	···	···	17.95	···
679	Ch53	···	···	···	20.72	···
679	Ch53	···	···	···	19.85	···
713	Ch53	···	···	12.39	···	···
730	Ch53	···	7.27	···	···	···
733	Ch53	···	7.26	···	17.21	···
743	Ch53	···	···	···	16.98	···
748	Ch53	···	···	···	···	18.95
750	Ch53	···	···	···	···	20.22
778	Ch53	···	···	11.66	···	···
929	Ch53	···	6.22	10.19	14.81	···
930	Ch53	···	6.38	···	···	···
932	Ch53	···	···	10.24	···	···
941	Ch53	···	···	···	14.77	···
943	Ch53	···	···	···	···	16.99
969	Ch53	···	···	···	···	16.80
971	Ch53	···	···	10.20	···	···
988	Ch53	···	5.86	···	···	···
989	Ch53	···	···	9.82	14.22	···
992	Ch53	···	6.30	···	···	···

TABLE III-11. Stopping powers of the gases hydrogen, oxygen, nitrogen, and air for protons in the energy range 30–1000 kev. [Stopping powers in (ev×cm²/atom)×10¹⁵.]

Proton energy (kev)	Reference	H_2	N_2	Air	O_2
20	Ph53	5.11	13.0	···	11.17
30	Ph53	5.58	14.5	···	13.0
30	Du52	5.84	16.1	15.5	···
30	We53	···	···	15.5	···
40	Ph53	6.14	15.4	···	13.9
40	Du52	6.25	17.1	16.48	15.2
40	We53	···	···	16.5	···
50	Ph53	6.51	16.2	···	14.7
50	Du52	6.43	17.8	17.16	16.4
50	We53	···	···	17.5	
60	Ph53	6.51	16.7	···	15.1
60	Du52	6.45	18.2	17.7	16.9
60	We53	···	···	17.5	···
70	Ph53	6.32	···	···	15.3
70	Du52	6.36	18.5	17.9	17.15
70	We53	···	···	16.8	···
80	Ph53	5.58	···	···	15.2
80	Du52	6.23	18.5	17.9	17.15
80	We53	···	···	17.2	···
90	Du52	6.04	18.25	17.72	17.25
90	We53	···	···	17.6	···
100	Du52	5.83	17.9	17.5	17.17
100	We53	···	···	17.3	···
150	Du52	4.70	16.1	15.98	16.13
150	We53	···	···	15.5	···
200	Du52	3.90	14.2	14.2	14.70
200	We53	···	···	13.5	···
245	We53	3.05	···	···	···
250	Du53	3.33	12.5	12.74	13.26
250	We53	···	···	12.3	···
300	Du52	2.91	11.2	11.56	11.99
300	We53	···	···	11.2	···
350	Du52	2.60	10.13	10.60	11.01
350	We53	···	···	10.3	···
400	Du52	2.35	9.34	9.79	10.23
400	We53	···	···	9.6	···
406	Ch53	···	9.30	···	···
406	Ch53	···	9.32	···	···
450	Du52	2.14	8.62	9.05	9.45
450	We53	···	···	8.9	···
452	Ch53	···	8.62	···	···
500	Du52	1.97	8.08	8.39	8.84
501	Ch53	···	8.42	···	···
502	Ch53	···	8.16	···	···
541	Ch53	···	7.62	···	···
550	Du52	1.82	7.61	7.9	8.38
600	Du52	1.70	7.21	7.51	7.91
648	Ch53	···	6.47	···	···
648	Ch53	···	6.87	···	···
716	Ch53	···	6.40	···	···
717	Ch53	···	6.15	···	···
748	Ch53	···	5.98	···	···
914	Ch53	···	5.09	···	···
942	Ch53	···	5.05	···	···
973	Ch53	···	4.80	···	···
974	Ch53	···	5.30	···	···
1001	Ch53	···	4.85	···	···

The energy analyzing device was a beam decelerator which had been previously developed for other work. The device measured the deceleration voltage which was required just to bring the charged ions of the beam to rest, a procedure which was possible because of the low voltages used in the experiment.

(d) *Measurements at the Ohio State University.*— Measurements of the stopping power of gaseous nitrogen, Ne, A, Kr, and Xe have been made at Ohio State University (Ch53) with protons from their van de Graaff generator. The energies lie in the interval 400 to 1000 kev. Details have not yet been published concerning the gas absorption cell used. The energy loss measurement was by the displaced resonance technique which they used in their foil measurements, and which was also used by Madsen (Sec. III-A).

2. *Results and Discussion of the Measurements on the Stopping Powers of Gases for Protons*

The results of various recent investigations of the stopping powers of gases for protons of energies 20–1000 kev are given in Tables III-10 to III-13. The Chicago group (We53) and the group at Pasadena (Du52) have each measured the stopping powers of argon and air for 30–450 kev protons, and there is remarkably good agreement between their results, which were taken in quite different geometries and with different energy analysis technique.

In general the results from the Ohio State group (Ch53) agree well with the Pasadena group where they overlap, but there is some discrepancy in the stopping power of xenon as measured in the two investigations. Near 450 kev the Ohio State values are some 10 percent less than those from Pasadena. Since most impurities in xenon would lower the stopping power of the mixture, in the absence of other information it would seem prudent to give the greater weight to the results showing higher stopping power, i.e., those from Pasadena.

The measurements from Los Alamos (Ph53) show a more systematic divergence from those of other investigations. In the case of the stopping power of argon

TABLE III-12. Stopping powers of various inorganic gases for protons in the energy range 20–600 kev. Molecular stopping powers in (ev×cm²/molecule)×10¹⁵.

Proton energy (kev)	Reference	NH_3	H_2O	NO	CO_2	N_2O	CCl_4
20	Ph53	···	21.4	···	30.9	···	104.2
30	Du52	29.7	···	···	···	···	···
30	Ph53	···	23.6	···	37.2	···	114.6
40	Du52	32.0	25.0	32.6	44.2	47.0	···
40	Ph53	···	26.1	···	41.1	···	128.4
50	Du52	33.6	26.1	34.5	46.8	48.6	···
50	Ph53	···	27.2	···	43.9	···	132.1
60	Du52	34.6	26.9	35.7	48.4	49.9	···
60	Ph53	···	27.7	···	45.0	···	134.0
80	Du52	34.4	27.6	36.6	50.2	50.9	···
80	Ph53	···	···	···	45.4	···	134
90	Du52	33.9	27.5	36.6	50.5	51.0	···
100	Du52	33.5	27.3	36.4	50.5	50.7	···
150	Du52	30.1	24.7	33.2	47.1	47.0	···
200	Du52	25.6	22.0	29.7	42.5	42.0	···
250	Du52	22.3	19.7	26.7	38.1	37.6	···
300	Du52	19.9	17.9	24.1	34.6	34.0	···
350	Du52	17.9	16.2	22.0	31.6	31.0	···
400	Du52	16.4	15.0	20.3	29.2	28.6	···
450	Du52	15.1	13.9	18.9	27.0	26.6	···
500	Du52	14.0	13.0	17.6	25.2	25.0	···
550	Du52	13.1	12.2	16.6	23.7	23.5	···
600	Du52	12.3	···	15.7	22.4	22.2	···

TABLE III-13. Stopping powers of certain organic gases for protons in the energy range 30–600 kev. Molecular stopping powers in (ev×cm²/molecule)×10¹⁵ (see reference Du52).

Proton energy (kev)	CH_4	C_2H_2	C_2H_4	C_6H_6
30	37.4	43.4	···	116.0
40	39.7	47.4	54.4	126.0
50	40.9	49.5	57.4	133.0
60	41.3	49.8	58.7	135.7
70	41.2	49.2	58.8	135.5
80	40.8	48.0	58.0	134.4
90	40.0	46.7	56.7	133.5
100	38.9	45.0	55.5	131.7
150	33.6	38.5	48.8	116.5
200	28.6	32.9	41.4	102.0
250	24.8	29.0	36.1	89.2
300	22.0	25.9	32.0	79.8
350	19.8	23.5	28.8	72.2
400	18.1	21.4	26.2	66.3
450	16.65	19.7	24.1	61.4
500	15.5	18.4	22.4	57.3
550	14.5	17.2	20.9	53.9
600	13.6	16.2	19.6	51.0

for protons, the Los Alamos results are always lower than the Chicago-Pasadena average, by amounts varying from 5 to 15 percent. The Los Alamos values for nitrogen and oxygen are also lower than the California values, by approximately the same percentage. Correspondence and discussion between the investigators involved has up to the present given no clear reason for the discrepancy. The close agreement on argon and air between the Chicago and Pasadena groups would seem, at present, to give superior weight to their results. The Los Alamos results on protons in helium and hydrogen gases are much closer to those resulting from the work of other investigators.

The question may be raised as to whether the energy losses measured in these experiments include those arising from all possible events in the gas. In the next sub-section of this report an argument will be presented indicating that these experiments, because of their good geometry, measure only those losses which are incurred in interactions with practically free electrons, and exclude those events in which a large momentum is transferred to an atom of the gas.

3. Stopping Powers of Gases for Particles Heavier than Protons

A Cockcroft-Walton accelerator or a van de Graaff generator will accelerate any positive ion which can be produced at its high-voltage electrode, and, using a low-voltage capillary arc, beams of He^+, N^+, Ne^+ ions are readily obtained. If, as in Weyl's apparatus (Fig. 11), there are no foils in the path of the beam, these ions can be passed through a gas in a differentially pumped chamber and the resultant degradations in energy studied. Thus, Weyl (We53) has obtained results on the loss of energy of ions heavier than protons which have passed through a gas without having undergone any large angle deflections. These results are shown in Table III-14.

In the experiments with these heavier ions, a phenomenon becomes outstanding which is already observable to a considerable extent with hydrogen beams, namely, the great diminution in intensity of the transmitted beam when gas is admitted to the absorption cell. This of course means that with the ions of higher Z the occurrence of nuclear scattering, with its large angular deviations and higher energy losses, is becoming more and more prevalent. The recent work at Oak Ridge (Ev53) shows clearly the marked spreading of the beam when such heavy ions are stopped in a gas.

Weyl's gas absorption tube was 74 cm long, 2.22 cm in internal diameter, and the entrance and exit apertures were circular, and 0.038 cm in diameter. Under these circumstances an event in the gas which deviated the ion as much as 5×10^{-4} radians from its direction of motion would remove it from the beam. Bohr's formula (Bo41) for the contribution to dE/dx from the screened nuclear, or "hard," collisions is

$$\left.\frac{dE}{dx}\right|_{\text{"hard"}} = \frac{4\pi e^4 z^2 Z^2}{Mv^2} \log\left(\frac{a^{\text{scr}}}{\mu v^2 / zZe^2}\right) \frac{\text{erg}\times\text{cm}^2}{\text{atom}}, \quad (19)$$

where z, Z are the atomic numbers of the moving particle and the stopping nucleus, respectively; M is now the atomic mass of the nucleus, and μ is the reduced mass of nucleus and particle; v is the velocity of the particle in cm/sec; and a^{scr} is the distance between particle and nucleus when the electronic screening has set a limit to the action of the nuclear charges. a^{scr} may be calculated with sufficient accuracy from the formula

$$a^{scr}=a_0(z^{-1}+Z^{-1}),$$

in which a_0 is the Bohr radius. The formula for losses by ionization of the medium has been given as Eq. (3). Although the square of the nuclear charge of the moving ion apparently appears in the numerator in the expression for both types of interaction, it is actually the ionic charge that is effective in ionization of the medium, and the nuclear charge that is effective in nuclear scattering. The latter is not energy-dependent, but in the electronic collisions we are dealing with a function of the ion energy which tends to zero at the lower velocities where the moving ion has been neutralized by the capture and retention of electrons from the stopping medium. Thus, for heavy moving ions of relatively high kinetic energy but low velocity, the loss of energy by "hard" collisions assumes much importance, although we must remember that even a neutral moving atom has a possibility of ionizing the medium, as pointed out above (Sec. II-D-1).

At kinetic energies of a few hundred kilovolts the moving ions of He, N, and Ne are to a considerable extent singly ionized; their effective Z for ionization of the medium lies between 0 and 2. Thus, we cannot neglect the contribution of "hard" scattering to the total energy loss in an experiment in poor geometry.

This means that if monoenergetic neon ions were liberated isotropically from a point in an atmosphere of argon gas, and note made of the average energy of the neon ions which passed in any direction through a spherical surface in the gas centered on the source, the stopping power of the argon gas would appear considerably greater than that observed in Weyl's experiments. Many of the neon ions would have suffered large angle deviations with high energy transfers to argon atoms within the spherical volume.

Calculation of the stopping power for hard collisions of neon ions in argon at 400 kev from Eq. (19) gives 15×10^{-15} ev×cm²/atom. Weyl's observed dE/dx from electronic collisions was 86×10^{-15} and at most 85 percent of this energy loss would go into a type of collision producing electronic excitation in the gas. It has been pointed out (Al53) that this may be a factor in explaining the lowered efficiency of heavy ions in producing scintillations (presumably by electronic enounters) in sensitized crystals.

The energy loss in hard collisions falls off rapidly as the deviation in the collision decreases, or, in other words, as the impact parameter increases. Bohr has shown (Bo48) that the contribution to dE/dx from the "hard" scattering may be neglected in cases in which the deviation in path of the ions is less than an angle θ_a', where this angle is given by

$$\theta_a'=s_{min}/a^{scr}, \tag{20}$$

where s_{min} is the closest approach of the two nuclei in a head-on collision and is given by

$$s_{min}=2zZe^2/\mu v^2, \tag{21}$$

TABLE III-14. Electronic stopping powers of various gases for helium, nitrogen, and neon ions.[a] Atomic stopping powers in (ev×cm²/atom)×10¹⁵.

Moving ion	Kinetic energy (kev)	Gas H_2	He	Air	Argon
	150	8.6	10.2	30.6	63.3
	175	9.4	11.0	43.3	57.0
	200	10.2	11.7	33.7	60.0
Helium	250	11.0	13.2	36.3	66.0
	300	11.4	14.4	38.5	71.0
	350	11.9	15.5	40.5	75.0
	400	12.3	16.7	42.3	79.0
	150	12.7	16.7	...	...
	175	13.3	17.7	...	...
	200	13.8	18.7	52.6	90
Nitrogen	250	15.2	20.5	59.0	102
	300	17.0	22.2	64.5	114
	350	17.7	23.7	70.0	125
	400	18.5	25.0	74.5	135
	150	...	10.5	...	...
	175	6.9	11.8	...	...
	200	7.3	12.8	...	63
Neon-20	250	7.9	14.3	46	70
	300	8.8	16.0	50.5	77
	350	9.6	17.5	54.5	83
	400	10.3	18.0	58	86

[a] See reference We53.

TABLE III-15. Conversion factors for expressing the stopping power of gases in various units.

Given units	Units desired				
	(kev×cm²)/mg	(ev×cm²)/atom		ergs/cm at N.T.P.[a]	kev/cm at N.T.P.
	H_2 1	1.673×10^{-18}		1.440×10^{-10}	0.0899
(kev×cm²)/mg	He 1	6.645		2.881×10^{-10}	0.1786
	Air 1	24.05		2.070×10^{-9}	1.293
	Argon 1	66.29		2.855×10^{-9}	1.782
	5.977×10^{17}	H_2 1		8.610×10^{7}	5.375×10^{16}
(ev×cm²)/atom	1.505	He 1		4.305	2.688
	0.4158	Air 1		8.610	5.375
	0.1508	Argon 1		4.305	2.688
	69.42×10^{8}	1.162×10^{-8}	H_2 1		6.243×10^{8}
erg/cm at N.T.P.	34.95	2.323	He 1		6.243
	4.828	1.162	Air 1		6.243
	3.498	2.323	Argon 1		6.243
	11.12	1.861×10^{-17}	1.602×10^{-9}	H_2 1	
kev/cm at N.T.P.	5.599	3.722	1.602	He 1	
	0.7734	1.861	1.602	Air 1	
	0.5612	3.722	1.602	Argon 1	

[a] N.T.P. means 0°C, 760-mm Hg.

where μ is the reduced mass of the two colliding atoms. For neon ions of 400-kev kinetic energy in argon we compute that $\theta_a' = 6.3\times10^{-2}$ radian. Since, as we have seen, an angular deviation greater than 5×10^{-4} radian would throw the ion out of Weyl's detecting system, it is, *a fortiori*, certain that only electronic impacts were involved in the stopping power he measured. Table III-16 gives an idea of the influence of the mass of the moving ion on the fraction of the energy loss due to "hard" collisions.

Another interesting feature of the results for the heavy ions is shown in the fact that, for example, the stopping power of helium gas is the same for helium or neon ions at 150-kev kinetic energy, although the nuclear charges of the moving ions differ by a factor of five. According to present theories, the proper independent variable to use in discussing stopping power is not the energy but the velocity. We should thus compare the electronic stopping power of helium gas for helium ions at 150 kev with its stopping for neon ions at 750 kev. If the effective Z's of the two moving ions were the same, the same electronic stopping power would be found. A rather hazardous extrapolation of the data would indicate that the stopping power of helium for 750-kev neon ions would lie between 25 and 30 (in units $(\text{ev}\times\text{cm}^2/\text{atom})\times10^{15}$), compared to the value of 10.2 observed for helium ions. The square root of the ratio, 1.6, might give an indication of the relative effective charges of neon and helium ions moving through helium gas with the same velocity (about 2.6×10^8 cm/sec). This highly qualitative comment is made with the thought of foreshadowing the kind of conclusion that may be drawn in the future if more abundant and more precise data become available.

If we compare the stopping power of hydrogen gas for nitrogen and neon ions we are studying a case in which the two moving ions have quite dissimilar outer electronic structures, in contrast to the two noble gas ions mentioned in the preceding paragraph. Nitrogen ions of 280-kev kinetic energy have the same velocity as do 400-kev neon ions (about 2×10^8 cm/sec). The stopping power of hydrogen gas for such nitrogen ions is observed to be 16 (in the above units), to be compared with 10.3 for neon ions of the same velocity. The higher stopping power for the lower atomic number must be due to the relatively loose structure of the outermost nitrogen electrons, in contrast to the relatively tightly bound noble gas structure of neon.

TABLE III-16. Estimate of the ratio of energy loss in hard collisions to that in electronic collisions in argon gas. (Estimates at 400-kev kinetic energy.)

Moving particle	$a^{scr}\times10^9$ cm	Computed dE/dx for "hard" collisions, $(\text{ev}\times\text{cm}^2)/\text{atom}\times10^{15}$	Observed dE/dx from electronic encounters	Ratio of "hard" to electronic losses
H	5.6	0.02	16	0.12
D	5.6	0.04	25	0.2
He	2.9	0.25	79	0.3
Ne	0.82	15.0	87	17.2

The charge exchange cycle, in which a moving charged ion captures and then loses an electron produces as its result a pair of ions in the stopping medium, and thus is a mode of transfer of energy from the moving ion to the gas. The cross sections for capture and loss of electrons by hydrogen beams in air are known through the work of the Chicago group (Mo50, Ri51, Ka51). These data on protons allow us to put a lower limit on the energy loss due to charge exchange in such cases. We shall estimate this loss in hydrogen and in air at an energy where the electron capture and loss cross sections are equal. This is 52 kev in hydrogen and 25 kev in air. At this energy the two cross sections are each 6.3×10^{-17} cm^2 in hydrogen and 24×10^{-17} cm^2 in air. Since only one-half of the ions at this energy are singly charged and can pick up an electron, we have to divide the above cross section by two. Multiplying this by the ionization potential, since at least this amount of energy must have been given up, leads to 0.49×10^{-15} $\text{ev}\times\text{cm}^2/\text{atom}$ in hydrogen and 1.8×10^{-15} as a lower limit to the energy losses by charge exchange in air. The total measured energy loss cross sections for protons in hydrogen and air are 6.4 and 14×10^{-15} (ev cm^2), respectively. Hence, the charge exchange phenomenon accounts for at least 7.7 percent of the observed stopping power of hydrogen gas for 52-kev protons, and 14 percent of that of air for 25-kev protons. At higher ion velocities the electron capture cross section decreases rapidly, and therefore the effect of charge exchange in the stopping of protons becomes negligible.

For the heavier ions, which move much more slowly at kinetic energy values equivalent to those of protons, charge exchange is certainly an important mechanism for energy transfer, but in the complete absence of data, speculation must be considered futile.

C. Capture and Loss of Electrons by Moving Ions in the Energy Range 20–7000 Kev

1. Reduction of Experimental Data to Cross Sections

An introductory statement (Sec. II-D) has already mentioned enough of the theory to motivate the following summary of experimental work. It is, however, necessary to give some analysis for the interpretation of observations in terms of collision cross sections. These cross sections will be expressed per atom of material through which the ions are passing; in the general form σ_{ij}, the initial index represents the number of electronic charges on the ion before the event, the final index the number after the event. Thus, σ_{01} applied to He ions concerns the loss of an electron by a moving neutral He atom, while $\sigma_{0\bar{1}}$ applied to H ions concerns the capture of an electron by a moving, neutral H atom.

Although the simplest independent variable to use in setting up equations concerning the effect would seem to be the distance along the path of the ion, experiments are almost always conducted by varying the pressure (p) in a vessel which encloses a constant length (l) along the path of the ion, as schematically represented in Fig. 14, and the equations given here will apply to the composition of a beam which is leaving such a variable pressure chamber.

The equations for capture and loss when only two charged states of the ion are concerned (0 and 1) were given at an early date by Wien (Rü33) and are reproduced here in terms of cross sections, rather than the mean free paths used more frequently in Wien's time.

In the first simple case we are concerned only with the two cross sections σ_{01} and σ_{10}. In the region above 20-kev kinetic energy charge exchange in a hydrogen beam should be describable in terms of these only since we may neglect the fraction of negative hydrogen ions

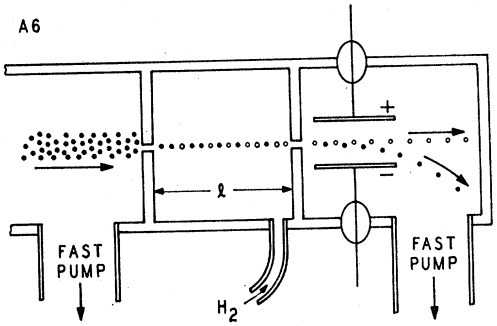

FIG. 14. Schematic representation of an experimental arrangement for the study of charge equilibrium in hydrogen ions passing through hydrogen gas. Neutral H atoms appear in the beam emerging from the charge exchange space of length l and the beam is then electrostatically analyzed. A similar setup was used by Snitzer (Sn53) with magnetic analysis and helium ions.

present (Ph53a, Ri51). Let n_1 be the flux of protons in the beam, n_0 the flux of neutral hydrogen atoms, $N=n_0+n_1$ the constant total flux of hydrogen, and $\pi=Ll\xi p/RT$ the measure of the number of gas atoms per square centimeter of the target. Here L is Avogadro's number, l the thickness of the gas target, ξ the number of atoms per molecule in the gas which is at pressure p, absolute temperature T; R is the gas constant 8.31×10^7 erg/mol C°. Then,

$$\begin{aligned} dn_0/d\pi &= n_1\sigma_{10}-n_0\sigma_{01}, \\ dn_1/d\pi &= -n_1\sigma_{10}+n_0\sigma_{01}, \end{aligned} \tag{22}$$

with solutions

$$\begin{aligned} n_1 &= \eta_1\exp[-\pi(\sigma_{01}+\sigma_{10})]+\eta_2, \\ n_0 &= -\eta_1\exp[-\pi(\sigma_{01}+\sigma_{10})]+\sigma_{10}\eta_2/\sigma_{01}, \end{aligned} \tag{22'}$$

where η_1, η_2 are constants of integration that will be deduced in the discussion of the various types of experiment.

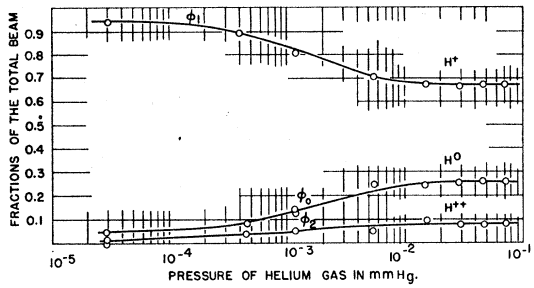

FIG. 15. Typical approach to equilibrium in the charge exchange process. This is 340-kev He^+ incident on He gas in the arrangement of Fig. 14 with $l=74$ cm.

In a system where there are three possible charge states, such as helium ions in motion, three simultaneous differential equations in n_0, n_1, n_2 can be written, of which two are independent because $n_0+n_1+n_2=N$. Here σ_{02} and σ_{20} correspond to events in which two electrons are transferred in a single encounter; while these are probably small compared to cross sections for single electron transfers, in the absence of experimental verification of this supposition they will be retained in the equations. Thus,

$$\begin{aligned} dn_1/d\pi &= n_0(\sigma_{01}-\sigma_{21})-n_1(\sigma_{21}+\sigma_{12}+\sigma_{10})+N\sigma_{21}; \\ dn_0/d\pi &= -n_0(\sigma_{01}+\sigma_{02}+\sigma_{20})+n_1(\sigma_{10}-\sigma_{20})+N\sigma_{20}; \\ n_2 &= N-n_0-n_1. \end{aligned} \tag{23}$$

The general solution of (23) can be obtained in a straightforward manner; in the special and interesting case where the boundary condition is such that for $\pi=0$, $n_1=N$, $n_0(0)=n_2(0)=0$, the solution may be written

$$\frac{n_1}{N}=\phi_1+(k_1e^{-q\pi}+k_2e^{q\pi})\exp\left(-\frac{\pi}{2}\sum\sigma_{if}\right).$$

$$\frac{n_0}{N}=\phi_0+\left(k_1\frac{q+S}{b}e^{-q\pi}-k_2\frac{q-S}{b}e^{q\pi}\right)\times\exp\left(-\frac{\pi}{2}\sum\sigma_{if}\right), \tag{23'}$$

where $2S=\sigma_{12}+\sigma_{21}+\sigma_{10}-\sigma_{01}-\sigma_{02}-\sigma_{20}$; $a=(\sigma_{01}-\sigma_{21})\times(\sigma_{10}-\sigma_{20})$; $b=\sigma_{01}-\sigma_{21}$; $q^2=S^2+a^2$; and $k_1=[(q-S)\times(N-\phi_1)-b\phi_0]/2q$; $k_2=[(q+S)(N-\phi_1)+b\phi_0]/2q$; and where ϕ_0, ϕ_1 are the limiting values of the beam fractions as π becomes large; these are the equilibrium values.

If a moving ion beam, homogeneous in velocity, impinges on a slab of matter and traverses it, a charge equilibrium is rapidly attained which is characterized by the set of fractions ϕ_i. Figure (15) shows the approach to equilibrium for a beam of helium ions, originally all He^+, as the pressure was increased in a charge exchange tube containing helium through which they were passed. In a tube length of 74 cm we see that equilibrium has been attained in the emergent beam when the pressure of the gas has reached 0.01-mm Hg.

TABLE III-17. Direct measurement of the equilibrium fraction of protons in hydrogen beams passing through hydrogen gas and air.[a]

Energy (kev)	ϕ_1 in Hydrogen	ϕ_1 in Air
20	0.231	0.405
30	0.315	0.500
40	0.419	0.545
50	0.500	···
59[a]	0.61	
60	0.56	
66.7[a]	0.67	
73.0[a]	0.73	

[a] a values are from reference Ri51, other values from reference Ba32. Values by Bartels are from a smooth curve through his data.

This approach to equilibrium is already shown in Eq. (23′) but for a simpler illustration, and for later use, we may continue the analysis of the hydrogen case whose general solution is Eq. (22′). In this set, put $n_0=0$ and $n_1=N$ for $\pi=0$ and obtain

$$\begin{aligned} n_1/N&=\phi_1+\phi_0\exp[-\pi(\sigma_{01}+\sigma_{10})],\\ n_0/N&=\phi_0(1-\exp[-\pi(\sigma_{01}+\sigma_{10})]), \end{aligned} \tag{22″}$$

where the ϕ's may be expressed as

$$\phi_1=\sigma_{01}/(\sigma_{01}+\sigma_{10}),\quad \phi_0=\sigma_{10}/(\sigma_{01}+\sigma_{10}). \tag{22‴}$$

The appearance of the sum of the capture and loss cross sections in (22″) is important because it illustrates that the rate of approach to equilibrium is governed by a cross section sum which is larger than the individual cross sections involved in the phenomena. It is a characteristic and simplifying feature of this process that charge equilibrium is attained in a variable pressure tube at pressures so low that no appreciable diminution of energy of the beam occurs in traversing the length of the tube. Thus, a mathematical treatment need not, at the present stage of experimental accuracy, concern itself with variation of the cross sections with velocity.

The variation of the various beam fractions with pressure for the case of three possible charge stages has already been given as Eqs. (23′), with the characteristic appearance of the sum of all possible cross sections. The equilibrium values ϕ_i may be expressed as

$$\begin{aligned} \phi_0&=[\sigma_{10}(\sigma_{21}+\sigma_{20})+\sigma_{20}\sigma_{12}]/D,\\ \phi_1&=[\sigma_{21}(\sigma_{02}+\sigma_{01})+\sigma_{01}\sigma_{20}]/D,\\ \phi_2&=[\sigma_{02}(\sigma_{10}+\sigma_{12})+\sigma_{12}\sigma_{01}]/D, \end{aligned} \tag{23″}$$

where

$$D=\sigma_{12}(\sigma_{01}+\sigma_{02}+\sigma_{20})+\sigma_{10}(\sigma_{21}+\sigma_{02}+\sigma_{20})+\sigma_{21}(\sigma_{01}+\sigma_{02})+\sigma_{01}\sigma_{20},$$

and if the cross sections involving double electron transfers may be neglected, these simplify to

$$\begin{aligned} \phi_0&=\sigma_{10}\sigma_{21}/D_0,\\ \phi_1&=\sigma_{01}\sigma_{21}/D_0,\\ \phi_2&=\sigma_{01}\sigma_{12}/D_0, \end{aligned} \tag{23‴}$$

where $D_0=\sigma_{01}(\sigma_{12}+\sigma_{21})+\sigma_{10}\sigma_{21}$.

2. *Experimental Values of the Equilibrium Fractions in Gases*

(*a*) *Hydrogen beams.*—The experimental work on this problem prior to 1933 has been summarized in (Rü33). The older work which seems most reliable in the energy range above 20 kev is that of Bartels (Ba30, Ba32). Other measurements by Meyer (Me37) do not agree as well with subsequent results.

Recently equilibrium fractions were measured by Ribe (Ri51) for hydrogen beams in hydrogen gas. In his work an initially nearly 100 percent pure proton beam was passed into a gas chamber in which the path length was 12.70 cm. The current collected from the proton constituent of the beam was measured in a Faraday cup and the decrease in this current noted as hydrogen gas was admitted into the chamber. Table III-17 gives the results of Bartels and of Ribe.

It is assumed, for the experiments leading to the values of Table III-17, that the current measured in the Faraday cup when there is no gas in the path of the beam gives the total beam flux N. If, however, this "zero" pressure beam contains some neutral atoms, caused by imperfect vacuum or neutralization of some protons on the walls of the beam-defining apertures, too small a total beam will be indicated, and the true fraction of the flux which is protons will be lower than that measured. If the individual cross sections σ_{10} and σ_{01} have been measured, the equilibrium fraction of protons can be calculated from Eq. (22‴). Ribe found a small systematic discrepancy between the directly measured equilibrium values of Table III-17 and those calculated from σ_{01} and σ_{10}, which was in the direction to be explained by the presence of a small neutral component of the "zero-pressure" beam.

Table III-18 gives computed values of ϕ_1 based on cross sections measured by the Chicago group (Mo50, Ri51 for hydrogen beams in hydrogen gas, and Ka51 for hydrogen beams in air). The equilibrium fractions for air have been calculated from formulas given by Kanner (Ka51) and quoted later in this section.

TABLE III-18. Equilibrium fractions of protons in a hydrogen ion beam in hydrogen and air, computed from measured capture and loss cross sections.

Energy in kev	ϕ_1 in H_2	ϕ_1 in Air
30	···	0.530
40	0.342	0.582
50	0.487	0.643
60	0.602	0.674
70	0.692	0.723
80	0.756	0.764
90	0.796	0.800
100	0.841	0.831
110	0.865	0.860
120	0.899	0.883
130	0.910	0.902
140	0.933	···
150	0.944	···

TABLE III-19. Equilibrium fractions of the various charged states in a helium ion beam traversing the gases H_2, He, Air, and Argon (Sn53).[a]

Ion energy (kv)	H_2 ϕ_0	ϕ_1	ϕ_2	He ϕ_0	ϕ_1	ϕ_2	Air ϕ_0	ϕ_1	ϕ_2	Argon ϕ_0	ϕ_1	ϕ_2
100	0.63	0.37	···	0.59	0.41	···	0.50	0.50	···	0.53	0.47	···
120	0.57	0.43	···	0.54	0.45	···	0.43	0.57	···	0.48	0.52	···
140	0.52	0.48	···	0.51	0.48	0.01	0.38	0.62	···	0.42	0.58	···
160	0.47	0.53	···	0.47	0.52	0.015	0.34	0.66	···	0.37	0.63	···
180	0.41	0.57	0.015	0.43	0.55	0.02	0.28	0.69	0.025	0.33	0.67	···
200	0.36	0.62	0.02	0.40	0.57	0.025	0.26	0.71	0.03	0.28	0.70	0.02
220	0.32	0.66	0.025	0.38	0.59	0.03	0.23	0.73	0.035	0.24	0.73	0.03
240	0.28	0.69	0.03	0.35	0.61	0.035	0.21	0.74	0.05	0.21	0.75	0.04
260	0.25	0.72	0.035	0.32	0.63	0.04	0.19	0.75	0.065	0.18	0.77	0.055
280	0.22	0.73	0.05	0.30	0.65	0.05	0.17	0.75	0.08	0.16	0.77	0.07
300	0.19	0.75	0.06	0.28	0.67	0.06	0.15	0.76	0.095	0.15	0.77	0.085
320	0.17	0.75	0.075	0.25	0.68	0.07	0.14	0.75	0.11	0.13	0.76	0.11
340	0.15	0.76	0.095	0.23	0.69	0.085	0.13	0.74	0.13	0.11	0.75	0.13
360	0.13	0.75	0.12	0.21	0.70	0.095	0.12	0.73	0.15	0.095	0.74	0.16
380	0.12	0.74	0.14	0.19	0.71	0.11	0.11	0.72	0.17	0.085	0.73	0.19
400	0.10	0.74	0.16	0.17	0.71	0.12	0.095	0.71	0.19	0.07	0.71	0.22
420	0.095	0.73	0.18	0.16	0.71	0.13	0.08	0.70	0.21	0.06	0.69	0.25
440	0.085	0.72	0.20	0.14	0.71	0.15	0.07	0.69	0.24	0.055	0.66	0.28
460	0.08	0.70	0.22	0.13	0.70	0.17	0.065	0.68	0.26	0.05	0.64	0.30
480	···	···	···	0.11	0.68	0.20	0.055	0.66	0.29	0.045	0.62	0.33

[a] ϕ_0 is the fraction of the total number of ions which is neutral at any time, and the subscripts 1 and 2 refer to He^+ and He^{++}, respectively.

(*b*) *Helium ions.*—A study of the charge equilibrium of a helium ion beam in the gases H_2, He, air, and argon has recently been published by Snitzer (Sn53). The original beam of He^+ ions obtained from a 500-kev Cockcroft-Walton accelerator or kevatron was passed through apparatus similar to that of Fig. 14, with magnetic deflection replacing electrostatic; the length of the tube was 74 cm. The equilibrated beam (with pressures of the order of 0.01 mm Hg) on leaving the tube passed into a circular chamber kept at high vacuum between the pole pieces of an electromagnet. This separated the three beam fractions by virtue of their different charge, and sent them through separate exit apertures; since the fractions all contained ions of the same average kinetic energy, a calorimetric measurement could be expected to indicate correctly the beam flux without requiring an investigation of the detector response to the charge of the particle incident on it. The use of such a detector is novel enough to warrant some descriptive detail.

Each beam fraction was detected on one of three identical targets. These consisted of a thin walled tube of nickel foil 0.0025 cm thick, 0.5 cm long and 0.3 cm in diameter. A No. 27A thermistor (a 0.05 cm diameter bead of a composition having a high temperature coefficient of electrical resistance) was placed on the axis of the foil tube and received heat by radiation from it. Ion beams of the order of 10^{-8} amperes produced temperature rises from 10–50°C at the various energies used. The lower values of the temperature rise ΔT were directly proportional to the power incident on the nickel foil; the higher values had a small radiation and conduction loss correction. This correction was determined as follows. The nickel tube targets were mounted on electrically insulating supports so that when one of the beams impinged on such a target a current flowed which was the sum of the rates of collection of positive charge from the beam and from the loss of secondary electrons, but which was directly proportional to the flux of ions in the beam. Thus, relative values of beam currents and temperature rises could be obtained by varying the kevatron beam at the same kinetic energy, and the losses thus were experimentally determined.

The results of Snitzer on the equilibrium fractions of He ions in various gases are given in Table III-19 and are shown graphically for air in Fig. 16.

As discussed briefly in Sec. II-D, one would expect than when the ratio $\gamma = v/v_0$ is of the order unity, the probabilities of capture and loss will be equal, and one-half of the moving ions will be neutral at a given moment. This expectation seems surprisingly well fulfilled for hydrogen and helium ions in air. The energy of a hydrogen ion beam at $\gamma = 1$ is 24.8 kev; for a helium ion beam it is 99.2 kev. At 25 kev the value of ϕ_1 for hydrogen ions in air is 0.50 from a slight extrapolation of Table III-18, and from Table III-19 we see that for helium ions in air ϕ_1 and ϕ_0 are 0.50 at 100 kev. For helium ions moving in hydrogen, helium, or argon gas the γ values for $\phi_1 = \phi_0 = 0.50$ range from 1.08 in argon

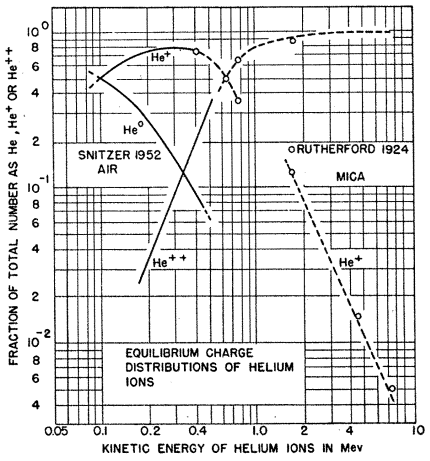

FIG. 16. Equilibrium charge fractions of He ions in air, including older results for He ions emerging from mica.

to 1.21 for helium or hydrogen gas. The largest discrepancy occurs in the case of hydrogen ions moving in hydrogen gas where the 50–50 point occurs at $\gamma=1.44$.

3. *Equilibrium Ratios on Emerging from Solids*

(*a*) *Hydrogen ions.*—The fraction of the hydrogen ions which are charged on emerging from metal foils in a vacuum has been investigated by Hall (Ha50). In his experiments protons in the energy region 20–400 kev were passed through a metal foil and, in the emergent, equilibrated beam the charged constituent could be deflected out of the beam by an electric field. The total equilibrated beam, or its neutral component, was measured by the scintillations caused in a KI(Tl) crystal, as detected by a photomultiplier tube. Since charge equilibrium is established after the penetration of a few atomic layers in the crystal, there can be no difference in its response to beams of originally neutral or charged hydrogen ions. The ratio of the photomultiplier currents with and without the electric deflection gives ϕ_0, the fraction of the total equilibrated beam which is neutral. Hall's results are given in Table III-20.

As we shall see below, in discussing charge equilibrium for emergent helium ions, most investigators have found that the composition of the equilibrium mixture is independent of the metal or solid in which it is produced. Hall found that he could not distinguish between the hydrogen in equilibria produced in beryllium, aluminum, and silver foils. The composition of the beam emergent from gold, however, contained more neutrals than beams from the lighter elements.

In discussing Hall's results, we may make the following remarks. His low-energy data did not take account of the possibility of H^- in the emergent beam. According to Phillips and Ribe (Ph53a and Ri51), about 4 percent of the equilibrated hydrogen beam may have been negatively charged at 20 kev. Also there is some doubt whether the entire equilibrating effect of a foil may not be due to a surface layer of foreign material. Such a layer, even if only between 5 and 10 atoms thick, would impress its own characteristic equilibrium on the emergent ions irrespective of the foil material. It is known that in the rather poor vacuum ($p\gtrsim10^{-6}$ mm Hg) used in this type of work, many metals take on a coating of absorbed oxygen, or even a layer of organic material from diffusion pump oil. Only very high vacuum techniques, such as the fresh evaporation of the foil material at pressures less than 10^{-8} mm, and its use as an equilibrating foil under baked-out high vacuum conditions would give one the right to assume that the effects of surface layers were being minimized. Such techniques have not, as yet, been applied in the work of the Chicago group.

TABLE III-20. Equilibrium fraction of protons (ϕ_1) in the total emergent hydrogen ion beam from metal foils.[a]

Hydrogen ion energy (kev)	Be, Al, or Ag foil ϕ_1	Au foil ϕ_1
25	0.56	0.56
50	0.68	0.68
74	0.75	0.75
99	0.82	0.80
124	0.87	0.85
149	0.909	0.886
174	0.939	0.910
198	0.954	0.935
223	0.968	0.952
248	0.976	0.968
298	(1−0.0159)	(1−0.0164)
347	(1−0.0113)	(1−0.0124)
397	(1−0.0050)	(1−0.0101)

[a] See reference Ha50.

(*b*) *Helium ions.*—Following the discovery by Henderson (He22) in 1922 that alpha particles emitted from a radioactive source and deviated in a magnetic field always show evidence of a singly as well as a doubly charged component, this phenomenon was the subject of several investigations at the Cavendish Laboratory and elsewhere (Ru24, Br27, He25, Ja27). Even from the bare source (RaC′) singly charged α particles were always found, and slowing down the particles by interposing a mica foil increased the fraction of singly charged ions. Detection was by counting scintillations on a ZnS screen after magnetic deflection of the particles. The work on natural alpha particles up to 1933 has been summarized by Geiger (Ge33).

Henderson (He25) extended the work of Rutherford on equilibrium produced in mica by using metal foils to slow down the particles. Except at the lowest energy used by Rutherford (405 kev), the equilibrium fraction of He^0 is so small that the ratio $n_1/(n_1+n_2)$ which may be computed from the experimental data, which give n_1/n_2, is not appreciably different from n_1/N, that is, from ϕ_1. Snitzer found $\phi_0=0.095$ for 400-kev helium ions in air and we have, in Table III-21, altered Rutherford's $n_1/n_2=0.75$ to $\phi_1=0.68$. We assume that the equilibrium mixture will contain approximately this same fraction of neutrals.

The results of Rutherford and of Henderson are summarized in Table III-21. The remarks made previously concerning the effect of foreign layers on the foil surfaces apply here but with less force, since at the relatively high energies of their work a thicker surface layer is needed to impress its characteristic equilibrium.

The charge composition of helium ions which have been scattered from a metal surface has been investigated by the Chicago group (Al53a) in some experiments as yet unpublished.

In these experiments a beam of monoenergetic He^+ ions was allowed to impinge upon thin and thick targets of gold, and a thick target of nickel. The helium ions scattered at 85°16′ from the beam, which struck the surfaces at a glancing angle of 45°, were examined in a spherical electrostatic analyzer for the ratio He^{++}/He^+.

TABLE III-21. The equilibrium fraction of He^+ in helium ions emerging from foils.[a]

Energy (kev)	Material	Reference	Fraction of total No. of helium ions which are singly charged
406	Mica	Ru24	0.68[b]
590	Mica	Ru24	0.60
640	Mica	Ru24	0.50
787	Mica	Ru24	0.346
1260	Mica	He25	0.156
1260	Gold	He25	0.137
1355	Mica	He25	0.138
1521	Silver	He25	0.116
1696	Mica	Ru24	0.12
1935	Mica	He25	0.0610
1935	Gold	He25	0.0654
2323	Aluminum	He25	0.0446
2408	Mica	He25	0.0389
2408	Mica	He25	0.0370
2408	Gold	He25	0.0415
2408	Gold	He25	0.0374
2719	Mica	He25	0.0325
2719	Gold	He25	0.0356
3406	Gold	He25	0.0235
4262	Copper	He25	0.0148
4440	Mica	Ru24	0.0150
4915	Mica	He25	0.0120
6028	Mica	He25	0.0079
6028	Gold	He25	0.0088
7680	As emitted from source on Pt wire	He25	0.0062
7680	As emitted from source	Ru24	0.0050

[a] See reference Ru24, He25.
[b] Rutherford's result was 0.75 for $He^+/(He^+ + He^{++})$; we assume that He^0 was present to about 10 percent.

The analyzer had such a large aperture that the electric currents arising from the transport of charge by the scattered ions were of the order 10^{-13} amperes and could be read on a recording electrometer. Charge equilibrium was established among the scattered helium ions *after* electrostatic deflection by interposing a foil in their path before their impact on the collecting probe. Thus, the same mixture of He^+ and He^{++} arrived at the probe irrespective of whether the charge on the analyzer was set for the transmission of the He^+ or He^{++} constituent. A NaI(Tl) scintillator was also used as a detector, the incident He^+ beam being depressed and reduced to the point where individual counting was possible. The data obtained from the NaI(Tl) detector and from the relative currents collected at the probe gave He^{++}/He^+ ratios which agreed to within 10 percent. Unfortunately, the method can give no information about neutrals, since it depends on electrostatic analysis, and in the energy range covered (150–450 kev) the fraction of neutrals cannot be ignored.

The ratio He^{++}/He^+ in scattered helium ions from metal surfaces is given in Fig. 17. It will be seen from Fig. 17 that the ratio He^{++}/He^+ in ions which have been charge equilibrated by scattering from a metal surface (nickel or gold) is considerably greater than when charge equilibrium has been produced by passage through air. There is considerable interest at present in the best method for producing multiply charged ions by stripping a moving ion beam; if these experiments are confirmed it would seem that, in this energy range, passage through a foil is considerably superior to equilibration in a gas for this purpose.

Snitzer's results for air, and Rutherford's for mica are shown in Fig. 16,|| || giving an idea of the behavior over the range 100–7000 kev. Rutherford measured his ratios He^+/He^{++} for helium ions emerging from mica and assumed that these would be the ratios at charge equilibrium in air. The present evidence would indicate that this is a questionable assumption, at least in the lower-energy region. It is seen that between its maximum value of about 0.75 in air at 300 kev, the fraction ϕ_1 has sunk by a factor of 150 to 5×10^{-3} at 7680 kev.

4. *Measurements of the Cross Sections for Capture and Loss of Electrons*

The equilibrium fractions discussed in the preceding section give ratios of the probabilities of capture and loss. In order to measure the probabilities separately, experiments involving the transient conditions, before equilibrium has been established, must be performed. Most of the measurements of individual cross sections have been made using one of the following methods.

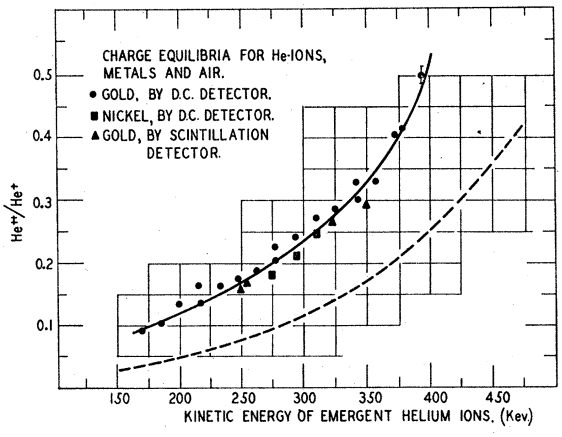

FIG. 17. Charge equilibria in He ions scattered by metals and transmitted by air.

|| || The Rutherford values were entered incorrectly in a similar figure (Fig. 7) in Snitzer's paper (see reference Sn53).

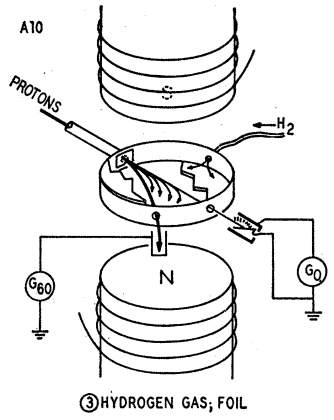

FIG. 18. Essentials of an experiment to measure σ_{01}, σ_{10} for hydrogen ions in hydrogen gas. Both beams decrease in intensity as gas is admitted. Any protons formed in the atomic beam are removed by the magnetic field and any atoms formed in the proton beam fly off tangentially (not shown).

(*a*) *Methods.*—(i) An arrangement similar to that of Fig. 14 is used. In a two component system, such as hydrogen ions above 20-kev kinetic energy, two measurements are carried out. The equilibrium fraction of protons ϕ_1, is measured by increasing the gas pressure until a pressure-independent mixture emerges from the tube. Then, at a lower pressure, before equilibrium has been established, a value of n_1/N is observed and the gas pressure noted. If one uses $\phi_0+\phi_1=1$ in Eqs. (22″), one finds these observations are sufficient for the calculation of the cross sections. This method was used by Bartels (Ba30).

(ii) The essentials of this second method are shown in Fig. 18, as applied to a situation in which one of the ionic states is neutral in charge. A mixed ion beam (produced, in the figure, by bringing the beam to charge equilibrium in its passage through a foil) is passed into a chamber which is in a strong magnetic field. The various charged states proceed through the chamber on orbits of different radii. A detector is placed on one of the beams, and gas is admitted to the chamber. There is a decrease in beam intensity because of the fact that when the charge of the moving ion changes due to capture or loss, the new ion moves on an orbit of different radius of curvature and is permanently lost from the beam. Thus, the new ion types are removed from the beam as fast as they are formed. If, for instance, a beam of neutral hydrogen atoms is under observation, the effect of method (ii) may be mathematically described as imposing the condition $n_1=0$ for all π in Eq. (22), leading to $dn_0/n_0 d\pi=-\sigma_{01}$, which means a simple exponential decrease in beam intensity as the pressure is increased. This method was apparently first used by Rutherford (Ru24), who produced the mixed beam by covering a RaC′ source with a mica foil and then observed σ_{12} for helium ions in air by noting the decrease of the He^+ beam as air was admitted to a deviation chamber in a magnetic field.

The method has recently been applied by the Chicago group (Mo50, Ri51, Ka51) to the study of σ_{10} and σ_{01} for hydrogen ions in hydrogen gas and in air.

Both methods (i) and (ii) impose rather arbitrary experimental definitions of the concepts "capture" and "loss." The only criterion established by the methods is that something has happened to the moving ion which changes the radius of curvature of its orbit in a magnetic field. Thus, "capture," as here observed, includes addition of an electron into an excited, and perhaps metastable, state of the resultant ion, but "loss" does not include events in which an electron in the moving ion

TABLE III-22. Experimental cross sections, in square centimeters, per atom of material traversed, for electron capture and loss.

Beam kinetic energy (kev)	Hydrogen beam in hydrogen gas		Hydrogen beam in air	
	Capture $\times 10^{17}$	Loss $\times 10^{17}$	Capture $\times 10^{17}$	Loss $\times 10^{17}$
31.4	...	...	20.8	...
34.0	15.2	...	...	...
38.2	17.6	...	...	...
40.6	...	...	16.0	...
40.8	...	...	...	24.4
41.4	...	...	...	23.1
43.0	...	...	15.6	...
44.5	9.1	6.7	...	...
48.3	7.6	...	...	...
48.7	7.0	...	...	...
49.4	...	...	13.4	...
50.8	...	6.4	...	...
53.9	5.7	...	...	...
55.7	...	...	11.6	...
56.6	...	...	11.5	...
58.1	...	...	10.1	...
62.5	3.8	...	...	...
63.0	...	...	9.7	...
65.6	...	...	9.3	...
67.0	...	...	...	22.2
70.5	...	5.7	...	...
73.0	2.8	...	6.8	...
77.0	...	...	7.1	...
81.1	1.8	...	...	...
88.8	1.4	...	...	...
103	0.84	...	...	...
105	...	...	...	20.8
107	...	...	...	21.0
109	0.74	...	...	...
112	...	4.7	...	...
114	...	...	3.4	...
117	...	...	2.7	20.6
120	0.48	...	...	...
122	...	...	2.7	...
123	...	4.3	...	...
128	0.41	...	...	...
142	...	...	...	19.8
149	0.23	...	...	...
153	...	3.8	...	...
156	...	...	...	18.8
193	...	...	...	17.4
204	...	3.2	...	...
252	...	...	...	14.4
263	...	2.8	...	...
280	...	...	...	14.5
305	...	2.4	...	...
321	...	2.3	...	...
325	...	...	...	13.6

is excited to a state which is bound. Thus, the role of the well-known highly metastable states in He I in these phenomena is still open for further experimentation, and this means that the light emitted by the moving ions must be investigated.

(*b*) *Capture and loss cross sections for hydrogen beams in hydrogen gas.*—The results of the Chicago group on hydrogen in charge exchange are shown in Table III-22 and Fig. 19. From these, it is clear that the capture and loss values are of the order of geometric atomic cross sections for $\gamma(=v/v_0)$ near unity since $\pi a_0^2=8.8\times10^{-17}$ cm^2, where a_0 is the Bohr radius.

For the case of hydrogen ions traversing air, Kanner found that his data on the cross sections per average air atom could be represented empirically as follows:

$$\sigma_{01}=(24.54-0.866E/E_0)\times10^{-17}\text{ cm}^2;$$
$$\sigma_{10}=41.1\exp(-0.562E/E_0)\times10^{-17}\text{ cm}^2; \quad (24)$$

and the equilibrium data of Table III-18 were computed (for air) from these equations. Here, $E_0=24.8$ kev; E is the kinetic energy in electron kilovolts.

The two cross sections behave quite differently with energy; in hydrogen Montague estimated that σ_{01} varies as $1/E^n$ where $n=0.70\pm0.05$. σ_{10}, however, has $n=3.5$, a fivefold increase in the magnitude of the exponent. Thus, a fast moving hydrogen atom is quickly stripped of its electron and has little probability of capturing another. We also note that the two probabilities for hydrogen ions in air are considerably larger at the same ion velocity (factors varying from 2.5 to 5) than they are in hydrogen gas.

(*c*) *Capture and loss cross section for helium ions.*—The experimental information at present available concerning capture and loss cross sections for helium ions is due to the work of Rutherford (Ru24) and some incidental observations of Snitzer (Sn53) in connection with his work on equilibrium fractions in helium.

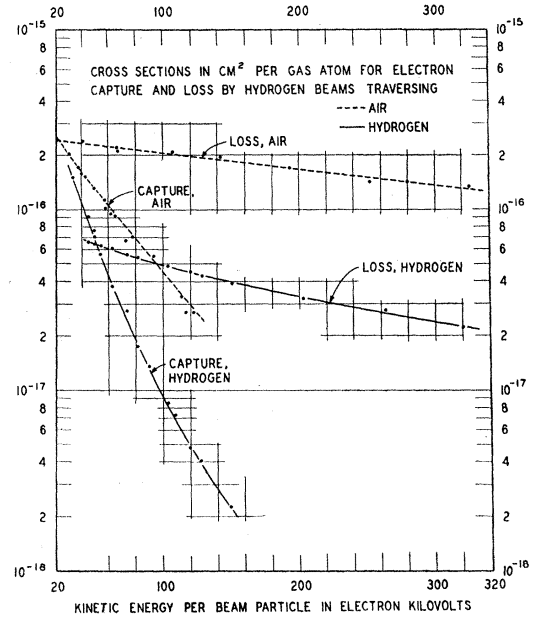

FIG. 19. Cross sections per atom of traversed gas for capture (σ_{10}) and loss (σ_{01}) of electrons by hydrogen ions in motion.

TABLE III-23. Some capture and loss cross sections for helium ions above 100 kev in kinetic energy.[a]

Energy kev	Gas		Cross section
131*	Helium	σ_{01}	1.72×10^{-16} cm^2 (±30%)
		σ_{10}	1.72×10^{-16} cm^2 (±30%)
340*	Helium	σ_{01}	8.3×10^{-17} cm^2 (±20%)
		σ_{10}	3.1×10^{-17} cm^2 (±20%)
		σ_{12}	1.4×10^{-17} cm^2 (±20%)
		σ_{21}	1.2×10^{-17} cm^2 (±20%)
646	Air	σ_{12}	6.2×10^{-17} cm^2
		σ_{21}	6.2×10^{-17} cm^2
1696	Air	σ_{12}	3.7×10^{-17} cm^2
		σ_{21}	5.01×10^{-18} cm^2
4440	Air	σ_{12}	2.38×10^{-17} cm^2
		σ_{21}	3.56×10^{-19} cm^2
6780	Air	σ_{12}	1.68×10^{-17} cm^2
		σ_{21}	8.43×10^{-20} cm^2

[a] Starred values from reference Sn53; other values from reference Ru24.

Rutherford obtained σ_{12}, the cross section per air atom for loss of an electron by He^+, using method (ii) as previously described. The mixed beam of various charge states was varied in energy from 650 to 6780 kev by using mica foils of different stopping powers over the RaC′ source. At these energies helium ions which have interacted with matter in their path are essentially only of the charge types He^+, He^{++}. Scintillations due to the He^+ beam were observed in a good vacuum; as air was admitted to the portion of the path in the magnetic field these diminished in number because of the process $He^+\rightarrow He^{++}+e^-$. This gave the mean free path or loss cross section σ_{12} directly for air. In order to obtain the capture cross section σ_{12}, Rutherford measured the equilibrium fractions in mica, and assumed that these same fractions would be applicable to air, which is somewhat questionable. On this assumption, he was able to compute σ_{21} for helium ions from the relation [see Eqs. (23‴)] $\sigma_{21}=\sigma_{12}\phi_1/\phi_2$. His results are given in Table III-23.

Snitzer, in his paper on the equilibrium fractions (Sn53), reports some tests of the attainment of equilibrium from which cross sections may be deduced. If the helium beam enters the gas chamber as He^+, the initial rates of growth of He^0 and He^{++}, and decay of He^+ may be found by imposing the conditions of (23′) for small, but not zero, values of π on Eq. (23). Then the initial part of the curves are given by

$$n_2/N=\pi\sigma_{12};$$
$$n_1/N=1-\pi(\sigma_{12}+\sigma_{10}); \quad (25)$$
$$n_0/N=\pi\sigma_{10}.$$

These equations serve to give estimates of σ_{12} and σ_{10} from the initial rates of change. Then from the equilibrium values, σ_{01} and σ_{21} may be calculated. This is clearly a slight modification of method (i), previously described.

Estimates of the cross sections applicable to helium ions at a few scattered energy values above 100 kev are given in Table III-23.

IV. HIGH-ENERGY MEASUREMENTS

In the high-energy region, measurements are unfortunately meager, with the methods necessarily differing somewhat from those used at low energies and, at least in the region above about 15 Mev, restricted to those few laboratories blessed with synchrocyclotrons. For purposes of verifying the theory, experiments have been largely concerned with the extraction of the value of I, the mean excitation potential, from the range and stopping power data; for use in other experimental work, the points on a range energy curve are sufficient.

Three forms of data are available. The absolute stopping power, or direct measurement of direct energy loss, consists of passing a well-collimated beam of known initial energy through a slab of stopping material of thickness Δx, determining the energy decrement ΔE, and calculating $\Delta E/\Delta x$. This corresponds to a popular practice at low energy except that magnetic analysis is most conveniently used for energy measurement, rather than electrostatic. From the value $\Delta E/\Delta x$, the value of I may be determined by fitting Eq. (3) to observation, and from a curve of dE/dx *vs* E, the range energy relation can be obtained as described in Sec. II.

The relative stopping power is determined by finding the thickness Δx_s of some standard substance (air at low energies, aluminum, copper at high energies) that reduces the beam energy the same amount as the thickness Δx of the material investigated. This can be done without actually measuring the energy loss, by sending the beam through just enough standard material to stop the particles, removing a known thickness and replacing the amount removed with enough thickness of the sample to produce the same effect near the end of the ionization (Bragg) or integral range curve. Then if we apply Eq. (3),

$$S=\frac{(Z/A)\ \log(2mv^2/I)-\log(1-\beta^2)-\beta^2}{(Z/A)_s \log(2mv^2/I_s)-\log(1-\beta^2)-\beta^2}$$

(mass stopping power),

in which the velocity v may be taken as the average velocity in Δx.

A. Methods

1. Berkeley

The data of the Berkeley group consist of the range measurements at 340 Mev (Ma51b) and the relative stopping power measurements by Bakker and Segrè (Ba51) and Thompson (Th52). With small modifications from one experiment to another the techniques were as follows.

(*a*) *Relative stopping power.*—The external beam of the synchrocyclotron—obtained either by electrostatic deflection or by scattering—was allowed to pass through a hole in the shielding material and collimated to diameters of the order of $\frac{1}{4}$ in.; a steering magnet then bent the beam (about 20°) into the cave area through, for example, a $\frac{1}{2}$-in. diameter×40-in. long collimating tube. In Thompson's work (see Fig. 20) the beam of

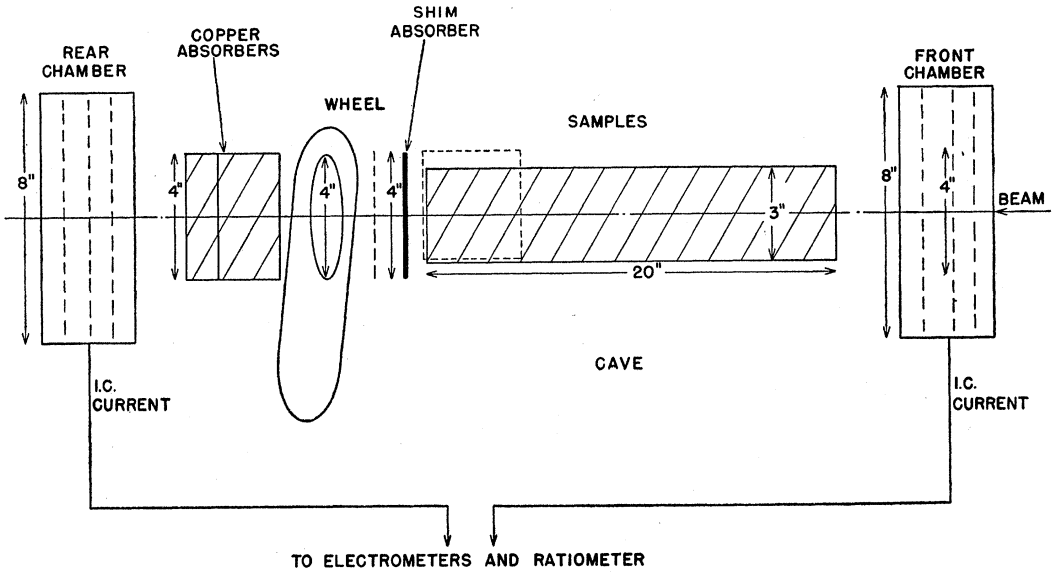

FIG. 20. Schematic of Thompson's (see reference Th52) apparatus for measurement of relative stopping power. The "shim absorbers" were used to make the energy loss in all the samples nearly equal.

protons first traversed a thin ionization chamber which served as a beam monitor; after this chamber the beam entered a sample of the material whose stopping properties were to be determined and following this an

". . . energy wheel with 12 slots containing step variations of copper of about 0.3 gm/cm² each. These were stamped with a circular die 4″ in diameter from 12.5 mil selected copper and carefully weighed. After the wheel was located a set of 4 absorbers working in a guillotine-like arrangement in such a way that any choice of these absorbers could be added or removed from the beam path by means of remote controls at a position outside the shielding. Next in the beam path were a predetermined number of copper blocks of 4″ square cross-sections and varying thickness. Each block was milled plane, flat and parallel to 0.2 mil and weighed to an accuracy of about 1 part in 50,000. Finally the rear ionization chamber was used to measure dE/dx near the end of the range."

The ratio of the currents from the two ionization chambers (read directly on an ingenious modification of a Leeds and Northrup Speedomax to a ratiometer) as a function of copper thickness respresented the raw data: the result is the end of the Bragg curve including the hump. The abscissa corresponding to 0.8 of the peak ionization value was then taken as the range in copper of the protons. With the thickness of the sample known precisely, and the measurement repeated with copper replacing the sample, the relative stopping power of the material could then be calculated.

(*b*) *Range.*—The range measurements (Ma51b) used roughly the same experimental arrangement (now with 1-in. collimation) with the addition that the beam first passed through Mather's (Ma51a) Čerenkov radiation apparatus, with which a precise measurement of the initial velocity of the beam could be made. After the beam energy was determined, the flux monitored, the beam passed through the copper absorber wheel, through a stack of plates of the metal being studied, and then into the second ionization chamber. The range is then given as the sum of the thickness of the main absorber and the equivalent thickness of the copper absorber wheel and chamber windows (less than 10 percent of the main absorber), this equivalence being calculated from (Ba51).

2. *Los Angeles*

(*a*) *Range.*—Hubbard and MacKenzie (Hu52) measured the range of 18-Mev protons in aluminum by using the internal beam of the 41-in. synchrocyclotron at UCLA. The beam was allowed to strike a heavy target on the median plane of the cyclotron and a fraction of the upward scattered component (the "axially scattered" beam) was used in the experiment. At a given azimuthal distance from the target, and above the median plane, a Faraday cage was interposed at an accurately known radius; in front of the cage, which was connected to an electronic electrometer, foils of aluminum were placed, one after another, in order to determine the absorber thickness that corresponded to a stoppage of one-half the beam. In this experiment, and in those of (Sa51 and Bl51), the beam energy could

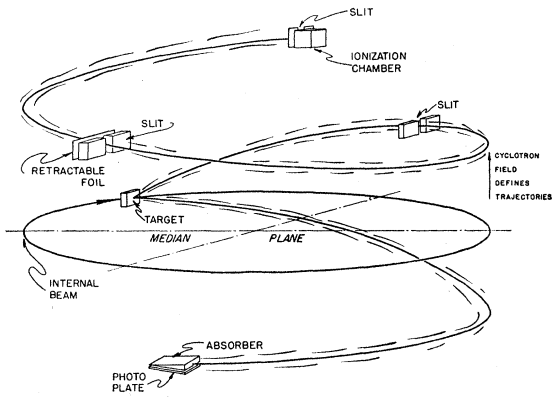

FIG. 21. Schematic illustrating internal beam cyclotron experiments. The "upper" experiment is similar to (Sa51), the "lower" to (Bl51).

be determined quite precisely since the magnetic field was referred in each case to the nuclear magnetic resonance frequency and the accuracy of the trajectory from target to detector is limited only by the patience of the plotter.¶¶

(*b*) *Absolute stopping power.*—The work of Sachs and Richardson (Sa51, Sa53) appears to be the first measurement of high-energy absolute stopping power. The cyclotron arrangement was similar to that of Hubbard and MacKenzie. They used the internal beam of the cyclotron, again with an axial deflection that allowed conveniently large intensities on the foil of stopping material and a precise value of the beam energy as measured by the cyclotron field itself. From the foil of high Z material (thorium) placed in the dee and on the median plane, those protons which multiply scattered upwards through angles small enough so that they were not captured by the dee, described a circular path inside the cyclotron, and 180° after scattering passed through a foil of the stopping material and then another 210° (20° past the scatterer, to take advantage of vertical focusing conditions in the cyclotron) to an ionization chamber detector whose radial position could be changed precisely from outside the vacuum tank. The shifts of radial position of the chamber with the foil "in" and "out" and a knowledge of the magnetic field along the trajectory (defined by a slit as in Fig. 21) then gave the energy loss in the foil.

3. *Harvard*

Again using the internal synchrocyclotron beam Bloembergen and van Heerden (Bl51) obtained the range-energy relation in aluminum, copper and lead, with an energy region stretching from 35–120 Mev. They used a tungsten scatterer (Fig. 21) and the down-

¶¶ In this connection it might be pointed out that a simple though somewhat less accurate method of determining the particle trajectory in an experiment of this type is the well-known floating wire method, described by J. Loeb, L'Onde Electrique **27**, 27 (1947) and L. Cranberg, AECU 1670.

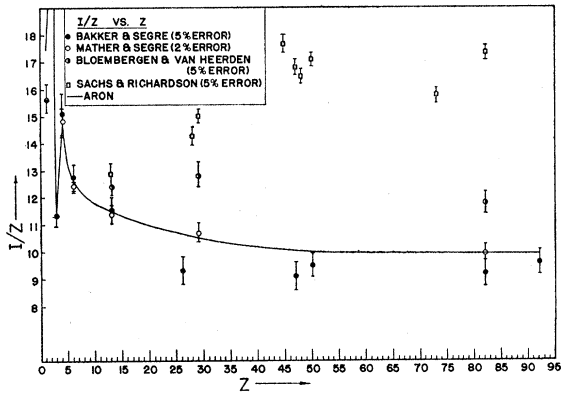

FIG. 22. Experimental determination of mean excitation potentials: I/Z *vs* Z. The errors given are orders of magnitude only.

ward scattered component was then detected by a photographic plate on a radius 180° after the scattering event; in front of the plate was a tapered absorber made of the stopping material. This absorber was made in the shape of a 30–60 triangular wedge, about 10-in. long, and the position of the absorber edge was located on the film with light marks. The photographic density along the direction parallel to the scattered beam, and at a given radius, then (after conversion by standard methods to particle flux) gave directly the integral absorption curve for an energy corresponding to the radius selected. Scanning the film in the direction perpendicular to the beam (along the cyclotron radius) yielded a measure of the energy spread in the beam, presumably resulting from the radial oscillation of the paths of the protons striking the target.

B. Experimental Results

From the total range (R) measurements (see Sec. II) the value of I can be calculated (Ar51) by using a trial value, I_1 from earlier experimental work, and computing the difference $R(I)-R(I_1)=R_{\text{exp}}-R(I_1)$. Aron, combining the results of a number of high-energy experiments and theoretical calculations, has calculated an extensive set of tables of dE/dx and range as a function of proton energy (Ar51). Since these tables represent the most definitive summary of experimental data taken up to the date of their calculation they can be used for comparison of subsequent data with theory. The smooth curve in Fig. 22 for the ratio I/Z *vs* Z gives the values used by Aron in his tables. Note that according to the Bloch theory I/Z should be constant for the heavy materials, and independent of incident particle energy. Hence, deviations from the theory should show up in a velocity-dependent excitation potential. It should be noted, of course, that the value of I is quite sensitive to errors in the observations, since in both the absolute and relative stopping power methods what is really determined is $\log I$ rather than I itself. In the absolute method, the relative error $\delta I/I$ is the stopping number B (say of the order of 10) times the relative error in the stopping power. Since a one percent error or greater in stopping is common, this means a five to ten percent error in the excitation potential derived from this data. The relation between range error and error in I is (Si52)

$$\delta R/R=\left[2+\frac{E}{R(dE/dR)}\right]\frac{\delta I}{I}.$$

In terms of the use of calculated tables for absorption measurements, this is fortunate, since the range values are therefore not sensitive to the chosen value of this parameter. For purposes of verifying the theory, it means that much more precise experiments will have to be done.

Experimental data for protons have been recently obtained at 10 Mev at Birmingham, at 18 Mev on the Los Angeles synchrocyclotron, between 35 and 120 Mev at Harvard, and at 340 Mev at Berkeley. At 10 Mev Simmons (Si52) using the external beam of the Birmingham cyclotron, scanned nuclear track plates (C2 emulsion) for range distribution of the proton beam after passing the beam through Al absorbers. Using Rotblatt's (Ro51) range-energy curve for the emulsion to determine the beam energy and Smith's range tables to convert to aluminum range, he found that Smith's range was about 0.8 percent too low and that $I_{\text{Al}}=155\pm3$ ev.

The principal result given by Sachs and Richardson is a list of ionization potentials fitted by the Bethe-Bloch equation. Their original values for aluminum differed only slightly (156 ± 3 ev compared with 150 ± 20 ev) from the value obtained by Wilson (Wi41) with a relative stopping power technique, but they later (Sa53) recomputed their I using more recent numbers for the fundamental constants with the result $I_{\text{Al}}=168\pm3$ ev, considerably different from both lower-energy values from absolute measurements (Warshaw-Kahn) and higher-energy values from relative measurements. The results of (Hu52) and (Bl51) should be of comparable accuracy since the techniques—at least for the energy measurement—were so similar. Thus, the low initial energy measurement is given with a stated error of 0.11 percent (18.00 ± 0.02 Mev), and the higher initial energy error is stated to vary from 0.2 percent to 0.3 percent. At 18 Mev the measured mean range is 477.0 ± 0.5 mg/cm² of aluminum, compared with 468.7 mg/cm² given in Aron's table. In the higher-energy region, there were smaller, but still significant deviations of the experimental from theoretical range*** of the order of about 1 percent greater than theoretical in the lower end. This results for both aluminum and copper.

For lead the experimental range was about 1 percent lower than theory. Note that the direction of the

*** While Bloembergen and van Heerden compared their data with the earlier tables of Smith (see reference Sm47), these are essentially identical with Aron's for aluminum.

deviation is the same in both of these last measurements although the magnitudes of the deviations are different.

Bloembergen and van Heerden computed the value of the mean excitation potential from their range data with the result that I_{exp} is considerably larger than that used by Aron. They give a corrected value for I_{Al} (the corrected I corresponding to the experimental range, in turn corrected for small angle scattering as in Sec. II) as 161 ev in the region 50 to 75 Mev and 164 ev in the region 75 to 120 Mev. Since the error in I_{Al} is about 5 ev, the difference is possibly not significant. Hubbard and MacKenzie get substantially the same corrected value for I_{Al}: 170±19 ev. Both of these values are therefore in essential agreement with the recomputed I_{Al} from Sach's data.

No data for energies greater than 340 Mev are at present available, although much work at this energy has been reported by the group at Berkeley. In the series of measurements by Bakker and Segrè (Ba51) the stopping power relative to aluminum of elements from H to U were determined, with the initial energy obtained from the orbit radius at deflection from the cyclotron. By use of the general method (Bragg curve) outlined above, the relative mass stopping power was measured to about 1 percent error (5 percent for hydrogen, obtained by a difference method using graphite and CH_2), thus yielding the ionization potential to about 5–10 percent if there were no errors in the value used for the potential of the standard substance (Al). For I_{Al} they used 150 ev from Wilson's (Wi41) data, which they stated was accurate to about 3 percent. A careful analysis of the pertinent data on air and aluminum has been made by Bogaardt and Koudijs (Bo51) who find that the best value for I_{air} in the region between 2 Mev and 10 Mev is 77.5 ev, rather than the 80.5 ev used by Wilson. Since Wilson's 150 ev for I_{Al} was based on the older value of I_{air}, they changed this to $I_{Al}=151\pm3$ ev, an increase small enough to discount in interpreting Bakker and Segrè's work. Agreement with the low-energy data of Madsen and Venkateswarlu could be taken to confirm the high-energy values (but see below).

Later in the same year, Mather and Segrè reported a set of range values for elements from Be to Pb, again using an ionization chamber for detection, and with the initial velocity of the protons (340 Mev) determined precisely by Mather's (Ma51a) Čerenkov counter method. Mean rectified range on the Bragg curve was taken at the distance (see Sec. II) where the ionization fell to 0.82 of its peak value.

Also at Berkeley, the results of Thompson's work on chemical additivity yields the ionization potential of H_2, C, N_2, O_2, Cl; these however, are based on stopping powers relative to copper, for which Thompson took $I_{Cu}=279$ ev, as in the work of Bakker and Segrè. The values of the mean excitation potentials obtained by the aforementioned authors are summarized in Table IV-2, and a summary of existing data is in Table IV-1.

TABLE IV-1. Summary of recent high-energy data.[a]

A. All elements

Element	Bakker-Segrè (Ba50) S(rel to Al) 340 Mev	Mather-Segrè (Ma51) Range (gm/cm²) 340 Mev	Thompson (Th52) S(rel to Al)[c] 270 Mev	Tobias, *et al.* (To49) S(rel to Al) 180-Mev deuterons	Bloembergen-van Heerden (Bl51) S(rel to Al) 70 Mev
H_2	2.634	···	2.605	2.57	···
Li	1.062	···	···	···	···
Be	1.024	76.73	···	1.02	···
C	1.124	70.03	1.137	1.12	···
N_2	···	···	1.126	1.10	···
O_2	···	···	1.108	1.08	···
Al	1.000[d]	79.02[b]	1.000[d]	1.000[d]	1.000[e]
Cl	···	···	0.999	···	···
Fe	0.906	···	···	0.889	···
Cu	0.875	91.8[b]	···	0.867	0.819
Ag	0.789	···	···	···	···
Sn	0.751	107.41	···	0.719	···
W	0.680	···	···	···	···
Pb	0.660	123.6	···	0.613	0.612
U	0.630	···	···	···	···

B. Results for aluminum

Observer	Initial energy (Mev)	I_{Al}(ev)	Method	Value
Simmons (Si52)	10	155±3	Range	0.1410+0.0001 gm/cm²
Sachs-Richardson (Sa53)	18	168±3	Abs. dE/dx	22.07±0.6 Mev/gm/cm²
Hubbard-MacKenzie (Hu52)	18	162±2.5	Range	0.4769±0.0005 gm/cm²
Bloembergen-van Heerden (Bl51)	66.1[f]	162±5	Range	4.774±0.008 gm/cm²
Mather-Segrè (Ma51)	340	147.9±3	Range	79.02±0.5 gm/cm²

[a] The complete data of (Sa52) were not given in their article.
[b] Average range for two energies differing by $<\frac{1}{2}$ percent.
[c] Converted from original as in Table II-2.
[d] Reference value.
[e] Actually Cu was the reference material; they also give experimental range as a function of energy from 35–120 Mev.
[f] Typical value of a set of energies.

TABLE IV-2. Summary of recent high-energy measurements of mean excitation potentials, I (ev).

Element	Z	Sachs-Richardson (Sa53) 18 Mev	Bloembergen-van Heerden (Bl51) 60 Mev[a]	Bakker-Segrè (Ba50) 340 Mev	Mather-Segrè (Ma51) 340 Mev[a]	Thompson (Th52) 270 Mev[e]
H	1	...	...	15.6[c]	...	18.0[d]
Li	3	...	...	34.0	...	...
Be	4	...	...	60.4	59.0	...
C	6	...	...	76.4	74.4	69.7
N	7	...	...	...	...	75.9[d]
O	8	...	...	...	...	87.6[d]
Al	13	168±3	162±5	150[b]	147.9±3	...
Cl	17	...	...	...	...	151.9
Fe	26	...	...	243	...	...
Ni	28	399	...	...	...	...
Co	29	435	370	279	309.9±3	...
Rh	45	799	...	...	...	...
Ag	47	796	...	428	...	...
Cd	48	792	...	...	...	...
Sn	50	853	...	479	...	...
Ta	73	1148	...	...	...	...
W	74	...	...	697	...	...
Au	79	1383	...	...	...	...
Pb	82	...	970	758	810.7±12	...
U	92	...	...	881	...	...

[a] Averaged over the several energies given in the original article.
[b] Taken as reference value, from Wilson.
[c] CH_2-carbon difference.
[d] Liquid target.
[e] These have been recalculated using Thompson's data and $I_{Al}=151$ ev.

The values of I/Z are also plotted in Fig. 22. Here it is seen that considerable deviations occur from the constancy of this quantity I/Z. These deviations, it has been noted by Sachs and Richardson (Sa53), cannot be explained by shell corrections and seem to give evidence of a velocity dependent I. Since each set of values reported was taken at a different energy, and with varying techniques, it would be more satisfactory to settle this question with data taken over a fairly large band of energies and with the same techniques. However, if it is granted that the variation in I is real, then some general tendencies are apparent.

It would then be advantageous to have some kind of semi-empirical method for obtaining the values of I for any Z and any energy. Lindhard and Scharf (Li52, 53) showed, using a dimensional argument and a Fermi-Thomas model, that the stopping number per electron, $B=(1/NZ)(dE/dx)(mv^2/4\pi e^4)$ (with the relativistic terms added to the right side when necessary), should be a function of Z/v^2 only. Following their suggestion, one may plot measured values of this quantity as a function of the logarithm of the dimensionless variable $x=v^2/v_0^2Z$, and the result should be a straight line if the Bloch formula is correct, with the log$x$ intercept giving the value of $I_0=I/Z$, or a smooth curve in any event. Figure 23 reproduces the curve from this paper, with the addition of points by Bloembergen and van Heerden and Thompson at high energy and Chilton, *et al.* at low energy. The curve is asymptotically straight (for $x\gtrsim 100$), and if the asymptote is projected back, the intercept gives $I_0=10.2$ ev. Then, if one writes $I=I_0Zf(x)$, $f(x)=\log(4Ryx/I_0)-B(x)$ and f may be determined from the figure. This has been done (only by taking graphical differences from the smooth curves shown) with the result given in Fig. 24. Evidently, as particle energy changes by a factor of 100, I changes by a factor of nearly 2. The maximum in the curve means also that a low-energy measurement of I may agree with one at high energy and still leave the intermediate energy stopping power not exactly calculable from the common result.

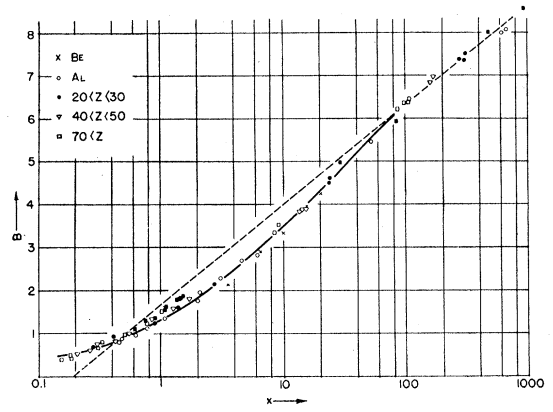

FIG. 23. $B(x)$, the experimental stopping number as a function of the variable $x=v^2/v_0^2Z$, reproduced from (Li53).

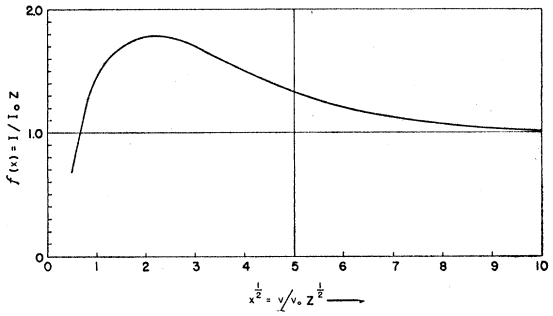

FIG. 24. The approximate energy variation of the mean excitation potential: $f(x)=I/I_0Z$ with $I_0=10.2$ ev.

BIBLIOGRAPHY

Al38 Allison, Skaggs, and Smith, Jr., Phys. Rev. **54**, 171 (1938).
Al53 S. K. Allison and Harvey Casson, Phys. Rev. **90**, 880 (1953).
Al53a Allison, Casson, and Weyl (to be published).
Ap51 R. K. Appleyard, Proc. Cambridge Phil. Soc. **47**, (2) 443 (1951).
Ar51 W. A. Aron, Thesis: "The Passage of Charged Particles Through Matter," University of California, (UCRL 1325).
Ba30 H. Bartels, Ann. Physik **6**, 957 (1930).
Ba32 H. Bartels, Ann. Physik **13**, 373 (1932).
Ba51 C. J. Bakker and E. Segre, Phys. Rev. **81**, 489 (1951).
Ba52 D. R. Bates and A. Dalgarno, Proc. Phys. Soc. (London) **A55**, 919 (1952).
Be51 Bernardini, Booth, and Lindenbaum, Phys. Rev. **82**, 307 (1951).
Be53 H. Bethe and J. Ashkin, *Experimental Nuclear Physics*, E. Segrè, editor. (John Wiley and Sons, Inc., New York, 1953), Chapter 2.
Be53a G. I. Bell, Phys. Rev. **90**, 548 (1953).
Bl33 F. Bloch, Ann. Physik. **16**, 285 (1933).
Bl51 Bloembergen and van Heerden, Phys. Rev. **83**, 561 (1951).

Bl49 O. Blunck and L. Leisegang, Z. Physik. **128**, 500 (1950).
Bø40 Bøgild, Brøstrøm, and Lauritsen, Math-fys. Medd. Acad. Copenhagen **18**, 4 (1940).
Bo41 N. Bohr, Phys. Rev. **59**, 270 (1941).
A.Bo49 A. Bohr, Kgl. Danske Videnskab. Selskab. Mat-fysk. Medd. **24**, 19 (1949).
Bo48 N. Bohr, Kgl. Danske Videnskab. Selskab. Mat-fysk. Medd. **18**, 8 (1948).
Bo51 M. Bogaardt and B. Koudijs, Physica **17**, 703 (1951).
Br27 G. H. Briggs, Proc. Roy. Soc. (London) **A114**, 241 (1927).
Br30 H. C. Brinkman and H. A. Kramer, Proc. Acad. Sci. Amsterdam **33**, 973 (1930).
Br41 Brunings, Knipp, and Teller, Phys. Rev. **60**, 657 (1941).
Br50 L. M. Brown, Phys. Rev. **79**, 297 (1950).
Br51 Browne, Craig, and Williamson, Rev. Sci. Instr. **22**, 952 (1951).
Ca52 D. O. Caldwell, Phys. Rev. **88**, 131 (1952).
Ca53 H. G. DeCarvalho and H. Yagoda, Phys. Rev. **88**, 273 (1953).
Ch53 Chilton, Cooper, and Harris, Bull. Am. Phys. Soc. **28**, 71 (1953).
Cr42 C. M. Crenshaw, Phys. Rev. **62**, 54 (1942).
Da14 C. G. Darwin, Phil. Mag. **27**, 499 (1914).
Di53 W. C. Dickinson and D. C. Dodder, Rev. Sci. Instr. **24**, 428 (1953).
Du52 Dunbar, Reynolds, Wenzel, and Whaling, Bull. Am. Phys. Soc. **27**, 6 (1952).
El52 Ellis, Rossi, and Failla, Phys. Rev. **86**, 562 (1952).
Ev53 Evans, Stier, and Barnett, Phys. Rev. **90**, 825 (1953).
Fe40 E. Fermi, Phys. Rev. **57**, 485 (1940).
Fe47 E. Fermi and E. Teller, Phys. Rev. **22**, 399 (1947).
Fr51 A. P. French and F. G. P. Seidl, Phil. Mag. **42**, 537 (1951).
Ge33 H. Geiger, Handbuch der Physik **22**/2, 221 (1933).
Gr50 Groetzinger, Berger, and Ribe, Phys. Rev. **77**, 584 (1950).
Gr52 A. C. Graves and D. K. Froman, *Miscellaneous Physical and Chemical Techniques of the Los Alamos Project* (McGraw-Hill Book Company, Inc., New York, 1952).
Ha38 G. T. Hatch, Phys. Rev. **54**, 165 (1938).
Ha48 O. Halpern and H. Hall, Phys. Rev. **73**, 477 (1948).
Ha49 T. A. Hall and S. D. Warshaw, Phys. Rev. **75**, 891 (1949).
Ha50 T. A. Hall, Phys. Rev. **79**, 509 (1950).
Ha51 Hanson, Lanzl, Lyman, and Scott, Phys. Rev. **84**, 634 (1951).
Ha52 E. L. Hubbard and K. R. MacKenzie, Phys. Rev. **85**, 107 (1952).
He22 G. H. Henderson, Proc. Roy. Soc. (London) **A102**, 496 (1922).
He25 G. H. Henderson, Proc. Roy. Soc. (London) **A109**, 157 (1925).
Hi48 J. O. Hirschfelder and J. L. Magee, Phys. Rev. **73**, 207 (1948).
Hu49 T. Huus and C. B. Madsen, Phys. Rev. **76**, 323 (1949).
Hu52 E. L. Hubbard and K. R. MacKenzie, Phys. Rev. **85**, 107 (1952).
Ig53 Igo, Clark, and Eisberg, Phys. Rev. **89**, 879 (1953).
Is50 I. Isenberg, Phys. Rev. **79**, 736 (1950).
Ja27 J. C. Jacobson, Nature **117**, 341 (1927).
Ja53 J. D. Jackson and H. Schiff, Phys. Rev. **89**, 359 (1953).
Ka51 H. Kanner, Phys. Rev. **84**, 1211 (1951).
Ka53 D. Kahn, Phys. Rev. **90**, 503 (1953).
Ki52 A. J. Kirschbaum, Thesis, University of California (Berkeley 1952) UCRL 1967.
Kn41 J. Knipp and E. Teller, Phys. Rev. **59**, 659 (1941).
Ko36 I. M. Kolthoff and E. B. Sandell, *Quantitative Inorganic Analysis* (Macmillan Company, New York, 1936), p. 306.
La44 W. Landau, J. Phys. (U.S.S.R.) **8**, 201 (1944).
Le52 L. Lewis, Phys. Rev. **85**, 20 (1952).
Li37 S. Livingston and H. A. Bethe, Revs. Modern Phys. **9**, 264 (1937).
Li52 J. Lindhard and M. Scharff, Phys. Rev. **85**, 1058 (1952).
Li53 J. Lindhard and M. Scharff, Kgl. Danske Videnskab. Selskab. Mat-fys Medd. **27**, 15 (1953).
Ma48a C. B. Madsen and P. Venkateswarlu, Phys. Rev. **74**, 648 (1948).
Ma48b C. B. Madsen and P. Venkateswarlu, Phys. Rev. **76**, 1782 (1948).
Ma51 R. Mather and E. Segrè, Phys. Rev. **84**, 191 (1951).
Ma53 M. Madsen, private communication.
Me37 H. Meyer, Ann. Physik **30**, 635 (1937).
Mi14 W. Michl, Sitzber. Akad. Wiss. Wein, Math-naturw. Kl. **123**, 1965 (1914).
Mo49 N. F. Mott and H. S. W. Massey, *The Theory of Atomic Collisions* (Oxford University Press, New York, 1949).
Mo50 J. Montague, Phys. Rev. **81**, 1026 (1950).
Mo51 G. Moliere, Z. Naturforsch. 3**a**, 78 (1948).
Pe52 A. M. Perry, Phys. Rev. **85**, 497 (1952).
Ph23 K. Phillip, Z. Physik **17**, 23 (1923).
Ph53 J. A. Phillips, Phys. Rev. **90**, 532 (1953).
Ph53a J. A. Phillips, Bull. Am. Phys. Soc. **28**, 31 (1953).
Ri51 F. Ribe, Phys. Rev. **83**, 1217 (1951).
Ro41 B. B. Rossi and K. I. Greisen, Revs. Modern Phys. **13**, 240 (1941).
Ro51 J. Rotblatt, Nature, **167**, 550 (1951).
Rü33 E. Rüchardt, Handbuch der Physik **22**/2, 103 (1933).
Ru24 E. Rutherford, Phil. Mag. **4**, 277 (1924).
Sa51 D. C. Sachs and J. R. Richardson, Phys. Rev. **83**, 834 (1951).
Sa53 D. C. Sachs and J. R. Richardson, Phys. Rev. **89**, 1165 (1953).
Sa52 G. A. Sawyer, Rev. Sci. Instr. **23**, 604 (1952).
Sc50 W. T. Scott and H. S. Snyder, Phys. Rev. **78**, 223 (1950).
Sc51 M. Schoenberg, Nuovo Cimento **8**, 159 (1951).
Sc52 W. T. Scott, Phys. Rev. **85**, 245 (1952).
Si52 D. H. Simmons, Proc. Phys. Soc. (London) **A65**, 454 (1952).
Sm47 J. H. Smith, Phys. Rev. **71**, 32 (1947).
Sn50 Snyder, Rubin, Fowler, and Lauritsen, Rev. Sci. Instr. **21**, 852 (1950).
Sn53 E. Snitzer, Phys. Rev. **89**, 1237 (1953).
St45 J. Strong, *Procedures in Experimental Physics* (Prentice-Hall, Inc., New York, 1945), Chapter 4.
St52 R. Sternheimer, Phys. Rev. **88**, 851 (1952).
Ta52 A. E. Taylor, Repts. Prog. in Phys. **15** (1952).
Th52 T. Thompson, Thesis, University of California (Berkeley 1952) UCRL 1910.
To45 S. Tolansky, Proc. Roy. Soc. (London) **A186**, 261 (1945).
To47 S. Tolansky, Proc. Roy. Soc. (London) **A191**, 182 (1947).
To51 C. Tobias, AECD-2099-A.
Wa49a S. D. Warshaw, Rev. Sci. Instr. **20**, 623 (1949).
Wa49b S. D. Warshaw, Phys. Rev. **76**, 1759 (1949).
Wa52 W. C. Walske, Phys. Rev. **88**, 1283 (1952).
We52 W. A. Wenzel and Ward Whaling, Phys. Rev. **87**, 499 (1952).
We53 P. K. Weyl, Phys. Rev. **91**, 289 (1953).
Wi41 R. R. Wilson, Phys. Rev. **60**, 749 (1941).
Wi47 R. R. Wilson, Phys. Rev. **71**, 385 (1947).
Wi48 H. A. Wilcox, Phys. Rev. **74**, 1743 (1948).
Wi45 E. J. Williams, Revs. Modern Phys. **17**, 217 (1945).